Final Report for AOARD Grant *104035*

Multi-Scale Investigation in the Nano-scale Mechanisms for Enhancing Strength and Interfacial Performance of Materials

Submitted to:
THE ASIAN OFFICE
OF AEROSPACE RESEARCH & DEVELOPMENT

Submitted by:

Department of Mechanical Engineering,
National Chung Cheng University

Yeau-Ren Jeng, Professor
Department of Mechanical Engineering,
National Chung Cheng University,
Ming-Hsiung, Chia-Yi 621,
TAIWAN

E-mail: imeyrj@ccu.edu.tw
Tel: 886-5-2428189
Fax: 886-5-2720589

Period of Performance: 16/03/2010 – 16/03/2011

Report Documentation Page

Form Approved
OMB No. 0704-0188

1. REPORT DATE	2. REPORT TYPE	3. DATES COVERED
30 MAR 2011	**Final**	**16-03-2010 to 15-03-2011**

4. TITLE AND SUBTITLE
Multi-Scale Investigation of the Nano-Scale Mechanisms for Enhancing Strength and Interfacial Performances of Materials

5a. CONTRACT NUMBER
FA23861014035

5b. GRANT NUMBER

5c. PROGRAM ELEMENT NUMBER

6. AUTHOR(S)
Yeau-Ren Jeng

5d. PROJECT NUMBER

5e. TASK NUMBER

5f. WORK UNIT NUMBER

7. PERFORMING ORGANIZATION NAME(S) AND ADDRESS(ES)
National Chung Cheng University,168 University Road, Ming-Hsiung,Chia-Yi 621,Taiwan,NA,NA

8. PERFORMING ORGANIZATION REPORT NUMBER
N/A

9. SPONSORING/MONITORING AGENCY NAME(S) AND ADDRESS(ES)
AOARD, UNIT 45002, APO, AP, 96338-5002

10. SPONSOR/MONITOR'S ACRONYM(S)
AOARD

11. SPONSOR/MONITOR'S REPORT NUMBER(S)
AOARD-104035

12. DISTRIBUTION/AVAILABILITY STATEMENT
Approved for public release; distribution unlimited

13. SUPPLEMENTARY NOTES

14. ABSTRACT
This is the report of a project to investigate nano-scale mechanisms and multi-scale behaviors of material systems made of nano-materials or nano/bulk-materials.

15. SUBJECT TERMS
Modelling & Simulation, multiscale modeling , Nanoscale mechanics

16. SECURITY CLASSIFICATION OF:			17. LIMITATION OF ABSTRACT	18. NUMBER OF PAGES	19a. NAME OF RESPONSIBLE PERSON
a. REPORT	b. ABSTRACT	c. THIS PAGE			
unclassified	**unclassified**	**unclassified**	**Same as Report (SAR)**	**65**	

Standard Form 298 (Rev. 8-98)
Prescribed by ANSI Std Z39-18

Abstract

This research is a concerted team effort to investigate nano-scale mechanisms and multi-scale behaviors of materials systems made of nano-materials or nano/bulk-materials. The fundamental understanding of nano-scale mechanisms is the key to the utilization of nano-materials and to the design of material systems contained nano-materials. The research program represents a synergistic effort to investigate different aspects of nano-scale mechanisms and multi-scale phenomena using the computational approaches by a team composed of researchers from AFRL-ML, NCCU of Taiwan and US universities.

Understanding major mechanisms affecting material strength such as grain size, grain orientation and dislocation mechanism from atomistic viewpoint can empower scientists and engineers with the capability to produce vastly strengthened materials. Mixed atomistic and continuum methods offer the possibility of carrying out simulations of material properties at both larger length scales and longer times than direct atomistic calculations. Our proposed innovative algorithm links atomistic and continuum models through the device of the finite element method which permits a reduction of the full set of atomistic degrees of freedom. This research gives a full description of the nano-mechanics approach with special multi-scale algorithm to the ways in which the method may be used to thoroughly study the deformation and strengthening mechanisms.

Our study has also performed experiments including depth-sensing indentation technique and *in-situ* pico-indentation to characterize the nano-mechanisms related to material strength and tribological performance. In this project, we have developed the innovative mutil-scale algorithms in the area of nano-mechanics. These approaches were used to studies the defect effect on the mechanical properties of thin film, mechanical properties of nanotubes, and tribological phenomena at nano-scale interfaces.

Introduction

Nanotechnology holds great promise to create novel materials that would have profound impact on the way people live their lives. A nano-system is usually made of nano-materials or nano/bulk-materials and thereby multi-scale in nature. A fundamental understanding of nano-scale mechanisms and multi-scale behaviors is the key to the utilization of nano-materials and to the design and fabrication of nano-systems. Moreover, the nanotechnology enabled multi-scale characterization of mechanical properties and interfacial phenomena to provide physical insight that was not available before and thereby lead to a multi-functional, robust, and durable nano-system.

The present research has developed multi-scale approaches that combine the models of different scales, effectively concentrating the computational power where it is needed the most to balance accuracy and efficiency. These approaches have then been used for the investigation of mechanical properties and interfacial phenomena of various nano-materials ranging from thin film, nanotubes to biomaterials. The present program represents a concerted team effort to investigate different aspects of multi-scale phenomena by a team composed of researchers from NCCU of Taiwan led by Professor Yeau-Ren Jeng. This team represents the core group working on multi-scale phenomena for AFOSR, in which the research has provided pioneering findings to lead to the ultimate goal of “material by design” from bottom-up approaches by including atomistic mechanisms.

This team has organized an international workshop on *Challenges in Computer Simulation*. The purpose of this workshop is to provide an international forum at which world leaders present and highlight thoroughly the most recent advances in atomistic and meso-scale modeling and how to bridge the time and distance scale gap. More recently, Prof. Jeng has been an invited as keynote speaker many international conferences and workshops, including *International Conference Multiscale Materials Modeling 2010 (MMM2010)* in Germany, *12th International Congress on Mesomechanics* in Taiwan, and *Cross-Strait Workshop on Nano Science & Technology (CSWNST-8)* in Hong Kong have been organized and focused on a comprehensive source of information on all areas of nanotechnology to the business, scientific and emerging computational algorithms. These workshops not only provided an opportunity for academic and industry professionals to discuss the latest issues related to advances in emerging nanotechnology, but also publicized good research and formed a network of knowledge and expertise.

I. Nano-scale Mechanisms for Material Strength

The material behavior under loading is subject to intensive investigation for centuries. It is well known that a wide range of materials properties are influenced significantly by the microstructures present in materials. A nano-system is usually made of nano-materials or various microstructures, e.g. dislocations [1], voids [2)], grains [3] and inclusions [4], after the manufacturing process. Once the sizes of the whole structures and the material microstructures become compatible, the microstructure effects on

the material behaviors become complicate and unexpected phenomena would start to appear, which could not be explained by tradition continuum theory.

For decades, scientists become to realize not only the compositions would affect the material properties, but also the microstructures of the compositions, e.g., grain size [5], grain orientation [6], and surface topology [7], etc. Microstructure effects on the mechanical properties of materials have been widely studied in micrometer range [8-10]. Grain sizes play a crucial role in work hardening behavior in metals [5]. Two classic papers on the relationship between grain size and yield strength were published independently by Hall [11] and Petch [12] and essentially the same conclusion were drawn that the yield strength is inversely proportional to the square root of the mean grain size. Taylor [13] formulated a model for the relationship between grain texture and mechanical properties and he assumed that the local deformation for each grain matched the global one neglecting the micro-mechanical interaction among grains. Following Taylor's full constraints model, various variants of relaxed constraints and self-consistent homogenization models were introduced which allow some of the strain constraints among the grains to be dropped [14-15]. These microstructures play an important role in the nucleation, evolution, and kinetics of larger defects, which eventually govern the macroscopic deformation and failure mechanisms observed in a variety of metals. Although the microstructure effects have been extensively investigated for years, a review of the published literature shows that the study on the effect of the microstructure in

nano-scale is still in its infancy stage. Some studies [16-18] suggest that the nano-crystalline materials exhibit reverse Hall-Petch effect, which is in contrast to the phenomena observed in micrometer scale. Latapie and Farkas [19] reported the effect of grain size on the elastic properties of nano-crystalline α-iron using atomistic simulations and a softening of the elastic properties is observed for grain sizes ranging from 12 nm down to 6 nm. Jeng and Tan [18] conducted atomistic simulations to show that nano-hardness of copper single crystal does not show the strong depth dependence as that in submicro-meter regime. A common fracture mechanism of ductile metals is nucleation, growth and coalescence of microscopic voids. Because of the critical role they play in the ductile fracture, voids in both metals and polymers have been subjected to extensive research over the last several decades. Shu [20] applied an elasto-viscoplastic strain gradient crystal plasticity formulation to study the deformation of a porous single crystal and its macroscopic stress carrying capacity under plane strain condition. It is found that both void growth rate and the local strain gradient decreased by several times when its radius is reduced to nano-sclae, which indicates that ``small'' voids are less susceptible to growth than `large' voids. Farrissey *et al* [21] conducted an atomistic study of void growth in single crystalline copper and the stress levels predicted for void growth are an order of magnitude higher than in the crystal plasticity model. It is suggested that the deformation mechanisms in nano-scale could be quite different from the one in micro-scale and, thus, more research effort is needed to reveal the underlying mechanisms. Moreover, the interaction effect between the structure size and microstructure especially in nanometer range, which few

studies were performed on, has been address in the present research.

The control of microstructure, which includes manipulating grain size, shape, orientation, composition, spatial distribution, etc, through physical models is of great interest in the development of new processes and products. Biological materials are remarkable examples of nature's ability to produce intricately complex compositions and structures. Elucidating the underlying principles selected by evolution can not only provide insight to imitate materials created by nature but also pave the way to the controlled design of materials with unprecedented properties. Recent development of nanotechnology holds great promise to create novel materials that would have profound impact on the way people live their lives. In order to design materials by manipulating their atomistic/molecular structures, the relationship between material atomistic structures and macro-properties need be established. Thus, it is essential to understand to deformation mechanism and distinguish the microstructure effects on the deformation mechanisms. The present program has developed both molecular simulation and multi-scale computational method to thoroughly study the deformation and strengthening mechanisms. Molecular simulation has been adopted to investigate the nano-mechanisms of microstructure while multi-scale technique was used to study the interaction between microstructure and structure size. Through this present algorithm, the micro-structure effect on the material properties can be comprehensively investigated so that innovative ideas based on the insight gained from this study has been demonstrated.

II. Nano-scale Interfacial Behaviors

All surfaces are microscopically rough. The real contact area exists between the contacting asperities of two surfaces pressed together under a normal load. The deformation of these contacting asperities plays a key role of in a variety of surface phenomena such as friction, adhesion, electrical, and thermal contact conductance, etc. The understanding of the single asperity contact is a fundamental step to investigate the contact behavior of rough surfaces, both at the microscale and the nano-scale. Many researchers have attempted to clarify the relationship between the roughness properties of two contact surfaces and the resulting stress and deformation. Kogut *et al.* [22] developed an elastoplastic model to describe the contact of an elastic, perfectly-plastic sphere with a rigid flat surface. Following their footstep, Jackson *et al.* [23] further account for the change in geometrical hardness caused by the evolving contact geometry and material properties, particularly in the fully plastic regime. Based on the molecular dynamics simulations, Luan and Robbins [24] showed that given an assumption of perfectly smooth atomistic-scale surfaces, the contact phenomena were in good agreement with those predicted by the Hertzian model. However, the atomistic roughness of the two surfaces broadens the distribution of the contact pressure between them, and thus causes the Hertzian continuum model to break down. The molecular dynamics simulation of a single asperity contact from Cha *et al*. [25] show that the force-displacement relationship exhibits a sawtooth form for dues to the repetitive generation and motion of partial dislocations. Although micro-contacts have been extensively investigated in recent years, a review of

the literature reveals that few studies have been performed using atomistic methodologies to examine the full range of asperity contact behavior; particularly those which take place beyond the elastic limit threshold or during elastoplastic deformation.

The tribological behavior is a complex and universal phenomena that is found at various sizes from the molecular scale up to the macro-scale. The deformation, surface roughness and contamination lead to various tribological mechanisms. It is well established that the adsorbed layers due to contamination plays a fundamental role in interfacial phenomena. Conventional tribological and lubrication techniques used for large objects can be ineffective at the nano-scale, which requires new physical insights for understandin interfacial behavior of nano-materials. Hence, it is with interests to clarify the mechanism of junction growth from nano-scale by an atomic simulation in energy minimizes method. Furthermore, nanoindentation and scanning probe microscopy are our primary testing methods to validate our researching the behavior of the entire real contact area of contacting bodies with real rough surfaces [10-13].

In this project, an approach which resembles FEM (Finite Element Method) methodology offers the possibility of carrying out simulations of material properties to locate the minimum-energy positions effectively [14-16]. Interactive forces within the contact area between surfaces play a pivotal role in tribological behaviors such as friction and adhesion. However the conventional finite element method cannot describe the atomic interactions. Since the primary concern of nano-interface is atom to atom interactions,

Molecular Dynamic (MD) is a suitable computational tool. Unfortunately, MD simulation is very time-consuming due to its large number of atoms and the large time scales involved in the simulated system. This present research is unique in that not only does it utilize the fact that the equilibrium position of the atoms of the condense matters, atoms or molecules is its minimum energy position but is also uses the FEM formulation to make the computational process efficient. The computation in this way is quasi-static, thereby greatly reducing the computation time. A multi-scale method that combine atomistic and continuum methods have been developed to offer the possibility to link two distinct length and time scales and implemented to carry out calculation of material properties that cannot be achieved by direct atomistic calculations alone. The developed method links atomistic and continuum models through the device of the finite element method which permits a reduction of the full set of atomistic degrees of freedom. Through this research, the underlying mechanisms that influence the material strength and tribological behavior have been thoroughly investigated so that a low energy consumption and durable system can be achieved to meet the compelling energy saving trend.

Approach

I. Nano-mechanics Computational Algorithm

In this approach, atoms are regarded as nodes, and their potentials are considered to be elements. It is assumed that atom, *i*, is located at position (x_i, y_i, z_i) with displacements u_i, v_i and w_i in the x- , y- and z-directions, respectively. By defining the nodal displacement vector for the *i* atom as $\{u\}_i$ and the corresponding external nodal force vector as $\{F\}_i = (f_i, g_i, h_i)^T$, the

total potential energy for atom, *i*, can be expressed as:

$$E_i = \frac{1}{2}\sum_{j\neq i}\phi\left(r_{ij}\right) + F\left(\sum_{j\neq i} f\left(r_{ij}\right)\right) - \left\{u\right\}_i^T\left\{F\right\}_i \tag{5}$$

where the atomic distance r_{ij} is given by:

$$r_{ij} = \left\{\left(x_i + u_i - x_j\right)^2 + \left(y_i + v_i - y_j\right)^2 + \left(z_i + w_i - z_j\right)^2\right\}^{1/2} \tag{6}$$

The differential of the atomic distance with respect to $\{u\}_i$ can be expressed as:

$$dr_{ij} = \frac{1}{r_{ij}}\left[x_i + u_i - x_j\ ,\ y_i + v_i - y_j\ , z_i + w_i - z_j\right] d\left\{u\right\}_i = \left[B\right] d\left\{u\right\}_i \tag{7}$$

The principle of minimum work enforces the minimization of the total energy of the whole system ($E_{total}=\sum_i E_i$) with respect to $\{u\}_i$ such that:

$$\frac{\partial E_{total}}{\partial\left\{u\right\}_i} = \sum_{j\neq i}\left[\frac{\partial F}{\partial\rho_i}\frac{\partial f}{\partial r_{ij}} + \frac{\partial F}{\partial\rho_j}\frac{\partial f}{\partial r_{ij}} + \frac{\partial\phi}{\partial r_{ij}}\right] - \left\{F\right\}_i = \left\{0\right\} \tag{8}$$

Equation (8) expresses the equilibrium equation at atom ***'i'***, which represents the equilibrium of the forces acting on atoms ***'i'***.

The unbalance force, $\{\xi\}_i$, can then be defined as:

$$\left\{\xi\right\}_i = \sum_{j\neq i}\left[\frac{\partial F}{\partial\rho_i}\frac{\partial f}{\partial r_{ij}} + \frac{\partial F}{\partial\rho_j}\frac{\partial f}{\partial r_{ij}} + \frac{\partial\phi}{\partial r_{ij}}\right] - \left\{F\right\}_i \tag{9}$$

In order to solve this nonlinear equilibrium equation in an efficient iterative way, it is necessary to differentiate $\{\xi\}_i$ with respect to $\{u\}_i$, i.e.

$$d\{\xi\}_i = \left\{ \begin{array}{l} \dfrac{\partial^2 F}{\partial \rho_i{}^2}\left(\sum_{j\neq i}\dfrac{\partial F}{\partial \rho_i}\dfrac{[B]}{r_{ij}}\right)\left(\sum_{j\neq i}\dfrac{\partial F}{\partial \rho_j}\dfrac{[B]^T}{r_{ij}}\right) \\ \quad + \sum_{j\neq i}\left\{\left(\dfrac{\partial F}{\partial \rho_i}+\dfrac{\partial F}{\partial \rho_j}\right)\left[\left(\dfrac{\partial^2 f}{\partial r_{ij}{}^2}-\dfrac{1}{r_{ij}}\dfrac{\partial f}{\partial r_{ij}}\right)[B][B]^T+\dfrac{1}{r_{ij}}\dfrac{\partial f}{r_{ij}}[I]\right]\right\} \\ \quad + \sum_{j\neq i}\left[\left(\dfrac{\partial^2 \phi}{\partial r_{ij}{}^2}-\dfrac{1}{r_{ij}}\dfrac{\partial \phi}{\partial r_{ij}}\right)[B][B]^T+\dfrac{1}{r_{ij}}\dfrac{\partial \phi}{r_{ij}}[I]\right] \end{array} \right\} d\{u\}_i \quad (10)$$

$$= [K_T]_i\, d\{u\}_i$$

Subsequently, the conventional finite element formulation assembly procedure can be employed to assemble Equation (8) in order to obtain the total system equation, i.e.

$$d\{\xi\} = [K_T]d\{u\} \quad (11)$$

Similarly, Equation (7) can be assembled to obtain the equilibrium equation of the total system, i.e.

$$\sum_i \xi_i = \{f\}_{\text{internal}} - \{F\}_{\text{external}} = \{0\} \quad (12)$$

In terms of the finite element formulation, Equation (11) represents the tangent stiffness equation, while the terms $\{f\}_{\text{internal}}$ and $\{F\}_{external}$ in Equation (12) denote the internal force vector and the external force vector, respectively. The simulation adopts the Newton-Raphson iterative technique to solve Equation (12) via the displacement control scheme or force control scheme. The need to calculate the full matrix of second derivatives in Newton-Raphson method can restrain the size of the simulated system. Therefore, the present research has developed an algorithm such as the utilization of the block-diagonal Newton-Raphson method to release this limitation. One of the challenges of nano-scale simulation is to predict the long-time system level performances. Hence, there is an imminent need to develop a multi-scale technique to bridge the gap between nano-scale and

micro-scale. In this follow-up project, the present research has also developed a coarse graining technique for the multi-scale simulation.

For the simulations of nano-scale thin film nanoindentation, the simulated system configurations include a perfect three-dimensional crystalline slab of atoms with a (001) surface, and an indenter has a triangular pyramidal form. In the simulation, it is assumed that the hardness of the indenter's diamond tip far exceeds that of the thin copper film. Hence the indenter deformation may be neglected during the indentation process. The simulation assumes boundary conditions in which the atoms located at the four sides and base of the simulated film are fully constrained. The interatomic potential of the substrate is modeled using the Sutton-Chen potential, which has the same functional form in an EAM potential as follows:

$$U = \sum_i U_i \tag{13}$$

$$U_i = \frac{1}{2}\sum_{j\neq i}\phi(r_{ij}) + F(\rho_i) = \varepsilon\left(\frac{1}{2}\sum_{j\neq i}\left(\frac{a}{r_{ij}}\right)^n - c\sqrt{\rho_i}\right) \tag{14}$$

where ρ_i is an electron density-like term for atom *i*, which is defined as:

$$\rho_i = \sum_{j\neq i} f(r_{ij}) = \sum_{j\neq i}\left(\frac{a}{r_{ij}}\right)^m \tag{15}$$

where r_{ij} is the distance between atoms *i* and *j*. The potential between the carbon and copper atoms is simulated using the Born-Mayer potential, which only produces an impulsive force. This potential has the following form:

$$\phi(r_{ij}) = A\exp[-2\alpha(r_{ij} - r_0)] \tag{16}$$

where r_{ij} is the distance between carbon atom *i* and substrate atom *j*. This modified-FEM approach is used to perform simulations of nanoindentation.

The distribution of the resulting stress and strain is then examined to clarify the atomic plastic behavior induced during the nanoindentation cycle. We also performed experiments using depth-sensing indentation technique. The load-depth curves of the experiments have been compared with those of computer simulation by the present approach. The indentation size effect and void effect are explored and discussed.

In addition, this study also utilizes molecular simulations to investigate the physical characteristics and the mechanical properties of carbon nanotubes (CNTs). The present research employs the Tersoff–Brenner many-body potential [26-28] to describe the inter-atomic forces, elastic properties, molecular bond energies, and bond lengths of the nanotubes. It has been used successfully by several researchers to model straight carbon nanotubes and to generate accurate predictions of the thermal properties of carbon nanotubes. The Tersoff–Brenner many-body potential is taken to have the form:

$$E = \sum_i E_i = \frac{1}{2}\sum_{i \neq j} V_{ij} \tag{17}$$

$$V_{ij} = f_c(r_{ij})[V_R(r_{ij}) + b_{ij} V_A(r_{ij})] \tag{18}$$

Here, E is the total energy of the system, which is decomposed for convenience into site energy E_i and a bond V_{ij}. The indices i and j run over the atoms of the system, and r_{ij} is the distance from atom i to atom j. The cutoff function, $f_c(r_{ij})$), is simply taken as

$$\begin{cases} 1, & r < R - D \end{cases}$$

$$f_c(r) = \frac{1}{2} - \frac{1}{2}\sin\left[\frac{\pi}{2}(r-R)/D\right], \quad R-D < r < R+D \tag{19}$$

$$0, \quad r > R+D$$

which has continuous value and derivative for all *r*, and goes from 1 to 0 in a small range around *R*. *R* is chosen to include only the first-neighbor shell for most structures of interest. The short range of the potential is numerically advantageous in many applications, and is important for the applicability of the simple ideas about coordination discussed here.

The potential itself contains a repulsive and an attractive part, V_R and V_A, that both have the exponential:

$$V_R(r) = A\exp^{-\lambda_1 r} \tag{20}$$

$$V_A(r) = B\exp^{-\lambda_2 r} \tag{21}$$

In the present work, b_{ij} is taken to have the following from:

$$b_{ij} = (1+\beta^n \xi_{ij})^{-1/2n} \tag{22}$$

where

$$\xi_{ij} = \sum_{k \neq i.j} f_c(r_{ik}) g(\theta_{ijk}) \exp[\lambda_3^3 (r_{ij} - r_{ik})^3] \tag{23}$$

$$g(\theta_{ijk}) = 1 + \frac{c^2}{d^2} - \frac{c^2}{[d^2 + (h - \cos\theta_{ijk})^2]} \tag{24}$$

where b_{ij} measures the relative strength of the attraction between atoms *i* and *j*, which depends on the parameters *β* and *n*, and the function, ξ_{ij}, which measures the total effect of all nearby atoms on the interaction. The $f_c(r_{ij})$ is again used to remove the effect of the more distant atoms from the calculation and the angular positions of the atoms are modeled with the function, $g(\theta_{ijk})$,

where θ_{ijk} is the angle between atoms *j* and *k*, measured from atom *i*, and the parameters *A*, *B*, λ_1, λ_2, λ_3, *c*, *d* and *h* are determined through fitting to experimental data. The present research systematically establishes a detailed definition of the mechanical properties of carbon nanotubes during the elastic and plastic deformation.

II. Clustered atomistic-continuum mechanics (CACM)

A novel clustered atomistic-continuum mechanics (CACM) based on the atomic mechanics and nonlinear transient finite element theory is proposed herein to simulate the mechanical behavior of the nano/bulk-structure under external mechanical loading or with thermal condition. In order to reduce the computational time efficiently and makes the simulation of the mechanical behavior of nano- and bulk- structure possible, the CACM treats the specific clustered atoms or molecule groups as a clustered super-element in the modeling, e.g. the sugar-phosphate backbone of DNA, super lattice of metal, and silicon. The cluster atom/molecule, namely super-atom/super-molecule should have the similar mechanical behavior with its discrete form. Moreover, the virtual super-element is adopted to describe the interaction energy/force between atoms or clustered-atom groups (e.g., hydrogen bond, covalent bond and other chemical bonds) via the atomic level potential energy and continuum mechanics. Furthermore, The Interfacial Element (TIE) has been introduced in CACM to bridge the interface of nano/bulk system, and with the capability of TIE, CACM should be able to tie nano and bulk (namely,

local-global) structures seamless in one multi-scale system. Finally, atoms, super-atoms and continuum mechanics based finite elements all were connected in one micro-macro (namely, local-global) simulation model using minimum energy technology. A typical CACM modeling is treated as clustered beam element with characters of axial forces, bending moments and torsions. The stacking energy between adjacent base pairs is essentially van der Waal force interaction which is described by the L-J potential form:

$$\phi(r_{ij}) = 4\varepsilon\,[\left(\frac{\sigma}{r_{ij}}\right)^{12} - \left(\frac{\sigma}{r_{ij}}\right)^{6}\,] \tag{25}$$

where ε is the depth of the potential well and σ is the (finite) distance at which the interparticle potential is zero and r is the distance between the particles. The molecular bonds between pairs are mechanically transferred into bending moments and forces which are expressed as:

$$F_j = \sum_i C_{(j,i)} \frac{\partial}{\partial x_i} E(R_0 + dx_i, \theta_0 + d\theta_i) \tag{26}$$

where *i*, *j* and $C_{(j,i)}$ represent the number of hydrogen bonds, different kinds of reaction forces/bending moments/torque and weighting coefficients. Note that x_j is displacment along the hydrogen bond direction. θ_j is the angle change between donor and acceptor, and $\theta_j = f_j(dx)$, where *f* is the specific function with respect to *j*. From theoretical, simulation results and computational efficiency aspects, CACM method can provide a feasible simulation technique to bridge the gap of atomistic and continuum mechanics. The CACM, an energy-based numerical analysis/prediction method adopted in this project is very flexible, effective, and robust, it is able to handle multi-scale, multi-loading simulation and process modeling applications which is not possible for any other existing methods.

Results and Discussion

- **The defect effects under nanoindentation**

Nanoindentation is an effective means of determining the mechanical properties of thin films and surfaces in nanometer regimes [29-30]. Computer simulation has attracted increasing interest in recent years as a technique for gaining valuable insights into the atomic processes associated with the nanoindentation cycle. Zimmerman et al. [31] conducted atomistic simulations to clarify the surface step effects on nanoindentation. Their results indicated that the yielding load decreases when indentation is performed in the vicinity of a surface step. Lilleodden et al. [32] conducted Atomistic simulations of elastic deformation and dislocation nucleation during nanoindentation. The results indicate that high angle grain boundaries are a ready source of dislocations in indentation-induced deformation. Knap and Ortiz [33] considered the effects of the indenter radius size on the nanoindentation of Au (001), and demonstrated that the indenter force is an unreliable indicator of the onset of dislocation for indenter sizes in the experimental range. A literature review reveals that previous studies have never addressed the nanoindentation of voided crystals. Although it is well known that even the purest real material contains a large number of defects within its crystal structure, it is impractical to simulate all of these defects at the atomic level. Hence, this study analyzes the interesting and computationally more straightforward problem of how the nanoindentation of Cu (111) crystal is influenced by the presence of a single void.

As one can see in Fig. 1, the outer normal direction of the upper surface of the slab is [111]. It is the stiffest direction in the copper lattice. Therefore it is expected that the 10–15% difference revealed in this study should be the more visible one than others in different orientations. The void depth in this study means the distance from the surface of the slab to the center of the void. Fig. 2(a) presents the variation in the load (i.e. the force experienced by the indenter) with the indentation depth for nanoindentation cycles performed with no void and with voids of three different sizes, respectively. Meanwhile,

Fig. 2(b) shows the load-depth curves for nanoindentation cycles performed with no void and with voids positioned at three different depths within the Cu slab, respectively. Fig. 2(a) demonstrates that, compared to the no void case, the presence of a void of any size leads to an enhanced displacement burst at an indentation depth of 0.55 nm and a 10–15% reduction in the magnitude of the maximum load. Table 1 lists the maximum loads and nanohardnesses obtained for the different void parameters considered in the present simulations. The nanohardness is computed by dividing the maximum load by the projected area of contact at that load. Table 1 demonstrates that a larger maximum load always corresponds to a larger nanohardness for the current simulation conditions. Hence, it can be concluded that the contact area is not influenced significantly by the presence of a void.

Fig. 3 shows the distributions of the hydrostatic stress and the von Mises stress induced at the maximum indentation depth in the cross-section of the indented copper substrate through the indenter tip and parallel with the (-101) plane. The results correspond to the case of no void and to the case of a void with a diameter of 1.2 nm and a depth of 1.5 nm. A comparison of the four subplots reveals that the distribution of the von Mises stress is not affected significantly by the presence of a void. However, the void does have a significant influence on the distribution of the hydrostatic stress. It can be seen that the stress accumulates at the internal surface of the void causing a reduction in the contact pressure. Fig. 4 presents the distributions of the hydrostatic stress for two different void parameters in the same cross-section as Fig. 3. Subplots (a)–(c) reveal the variation of the hydrostatic stress distribution with the void size, while subplots (d)–(f) illustrate the variation of the hydrostatic stress distribution with the void depth. It is observed in subplots (a) and (d) that although the void disappears, a stress concentration remains at the original void location. The disappearance of the void is to be expected since in these two cases, the indentation depth is sufficiently large to cause many surrounding atoms to slip into the void vacancy. The remaining subplots of Fig. 4 all reveal that stress accumulates at the internal surface of the void. The stress accumulation causes a reduction in the contact pressure

and prompts the void to deform into an elliptical shape. A stress reduction in the contact area is consistent with the maximum load reduction observed when a void exists in the substrate. In order to explore the influence of a void on the deformation mechanisms in nanoindentation, the dislocation structure in the substrate can be analyzed by performing a slip vector calculation at each atomic site. This quantity gives the Burgers vector for the slip of adjacent atomic planes, where the atom lies on one of these planes. It has a large magnitude for any inhomogeneous deformation near an atom and provide information regarding the deformation.

In order to explore the influence of a void on the deformation mechanisms in nanoindentation, the dislocation structure in the substrate can be analyzed by performing a slip vector calculation at each atomic site. This quantity gives the Burgers vector for the slip of adjacent atomic planes, where the atom lies on one of these planes. It has a large magnitude for any inhomogeneous deformation near an atom and provide information regarding the deformation. Fig. 5 presents scatter plots of the distributions of the slip vector norms at the maximum indentation depth as viewed from four different directions. In this figure, the results relate to the no void case. The observed dislocation structures resemble four-sided pyramids, whose sides lie parallel to the four different sets of {111} planes. This finding is reasonable since slip is known to occur along the close-packed {111} planes in FCC crystalline structures. The slip vector norms indicated in green correspond to 1.47 Å, which is very close to the value of a <112> partial dislocation in copper. Furthermore, the slip vector norm value of the atoms indicated in red is 2.56 A, which is consistent with the magnitude of a h110i perfect dislocation. Fig. 6 presents the corresponding scatter plots of the distributions of the slip vector norms at the maximum indentation depth for the case where the Cu slab contains a void of diameter 1.2 nm and a depth of 1.5 nm. A comparison of Figs. 5 and 6 confirms that the dislocation structure is not influenced significantly by the presence of a void. This finding provides a reasonable explanation for the earlier conclusion that the contact area is unaffected by the existence of a void.

The simulation results have presented atomistic simulations of the previously unexplored question of how nanoindentation is influenced by the presence of a void. Stress analysis has explained the observed reduction in maximum load caused by a void. Meanwhile, observation of the dislocation structure by means of slip vector analysis has shown that deformation in nanoindentation is not influenced significantly by the presence of a void. However, the cases simulated in this study have revealed that the existence of a void causes a reduction in the magnitude of the nanohardness by the order of approximately 10–15%.

- **Amophization in load rate dependent nanoindentation studies of crystalline silicon**

Indentation at very low load rate showed region of constant volume with releasing load in crystalline (*c*-) Si, indicating a significant observation of liquid-like amorphous phase which is incompressible under pressure. The molecular dynamic simulation has been employed to demonstrate that the effect of indentation velocities has a direct influence on *c*-Si during nanoindentation processes. In this study, amorphization has also been confirmed from load dependent indentation where increased amount of amorphized phase is made responsible for the increasing elastic recovery of the sample with increasing load.

In order to examine the influences of strain rates on the mechanical properties of the silicon film under nanoindentation, the simulations are performed using various indentation velocities ranging from 40 to 100 ms^{-1}. The present molecular dynamic simulations adopt the Tersoff potential [26-28] to study mechanical properties of silicon crystal with the (111) plane on the nanoindentation by solving the Hamilton equations of motion using Gear's fifth predictor-corrector method. Meanwhile, the *NVT* model is used to control the number of atoms *N*, the volume *V*, and the temperature *T*. Fig. 7 presents four nanoindentation load-displacement curves obtained when indenting silicon samples with the different indentation velocities of *V*=40, 60, 80, and 100 ms^{-1}. It is apparent that the effect of indentation velocities has a direct effect

on the initial slope of the load-displacement curves of the various silicon samples. Specifically, for a constant indentation force, the indentation depth reduces as the indentation velocity decreases, which implies that the mechanical strength of the silicon samples increases with a reducing indentation velocity. This phenomenon arises as a result of an increase in strain energies as the indentation velocity increases, creating an increasing number of dislocations (see Figs. 7(a) and 7(b)), and thereby in turn decreases the mechanical stiffness of the silicon specimen. Remarkably, Figs. 7(a) and 7(b) also shows that the crystalline phase of silicon samples transform continuously to an amorphous phase, which implies a dramatic change in atomic shortrange order by application of sufficiently large strain rates. It is necessary to note that the experimental loading-unloading rate is many orders of magnitude slower than the current simulation rate, which is comparable to that used in other MD simulations. Due to the computational intensity of the congenital problem, many of these simulations were restricted to smaller model sizes or to very high loading rates, or to both. In MD simulation, the model has orderly arrangement for atomic position to be consistent with crystalline structure. In contrast, the current results show a great number of disordered atoms, which implies liquidlike behavior.

- **Molecular simulations for characterising the mechanical properties of carbon nanotubes**

Since their original discovery by Iijima in 1991 [34], carbon nanotubes (CNTs) have attracted intensive interest throughout industry and academia. Experimental studies has shown that CNTs exist in a variety of structural configurations, including single-walled carbon nanotubes (SWCNTs) [35], multi-walled carbon nanotubes (MWCNTs) [36], bundles [37] and nanoropes [38]. As a result, CNTs have been extensively deployed in recent years for such diverse applications as memory chips, sensors, probes, tips, and reinforcement phase in composite materials. However, the nanoscale dimensions of CNTs prevent the use of direct experimental techniques for measuring their mechanical properties, and thus theoretical computational

simulations have emerged as the method of choice for characterizing their mechanical properties and obtaining detailed insights into the physical mechanisms governing their deformation. Of the various computational techniques available, one of the most commonly adopted is that of MD simulations. Due to the availability of accurate inter-atomic potential data for a wide range of common engineering materials, MD simulations, in which the material of interest is modeled at the atomic level, provide a powerful technique for clarifying a wide range of complex physical phenomena in the microscale and nanoscale regimes. MD simulations assume that the instantaneous positions and velocities of the individual atoms within the system of interest conform to the principles of Newtonian mechanics, and thus the dynamic history of the assembly and the energy and force of the system are generated by numerically integrating the equations of motion of each atom at each time-step of the simulation procedure. Although MD simulations are commonly regarded as an ideal means of analyzing the mechanical response of engineering materials at the micro- or nanoscale, great care must be taken when specifying the simulation parameters in order to ensure the validity of the numerical results. Moreover, due to the complexity of the MD computations and the large time scales considered in most simulation systems, the application of MD simulations to large-scale systems comprising many hundreds or thousands of atoms is impractical if not completely unfeasible.

In MD simulations, it is assumed that the majority of the atoms move freely throughout the body of interest in accordance with Newton's law of motion. However, in condensed matter, the atoms and molecules actually oscillate thermodynamically around their minimum energy positions, i.e. they have a quasi-static rather than dynamic characteristic. Accordingly, in recent years, a new class of simulation technique known as molecular statics (MS) has emerged [39], in which the final relaxed configuration of the atomic structure is determined using an energy minimization technique. Studies have shown that the quasi-static characteristics of MS simulations yield a considerable improvement in the computational efficiency compared to that of

MD simulations since the velocity components of the individual atoms within the system are ignored. As a result, the MS simulation approach has been increasingly employed in recent years as a means of gaining insights into the crystal lattice structure of common engineering materials under various conditions [40-42]. In practice, the choice of an appropriate molecular simulation approach (i.e. MD or MS) frequently comes down to a subjective decision on the part of the practitioner as to which technique can be expected to produce the most realistic results at an acceptable computational cost. Unfortunately, a review of the published literature reveals that no previous studies have utilized MS simulations to investigate the structural deformation of CNTs beyond their elastic limit during uniaxial deformation. In this project, this study performs a series of MS simulations using the Tersoff potential model [26-28] to investigate the respective effects of the wrapping angle and the tube on the tensile strength, bond length and bond angle of various zigzag and armchair SWCNTs. The applicability of the MS simulation approach is confirmed by comparing the simulations results obtained for the stress-strain response of the SWCNTs with those obtained using a conventional MD simulation technique.

Fig. 8(a) illustrates the variation of the tensile stress with the tensile strain in a zigzag (10,0) SWCNT as computed by the MS and MD simulation methods, respectively. It can be seen that the tensile stress of the SWCNT is clearly a function of the applied strain.. It can be seen that each of the three stress–strain curves has four distinct stages. In Stage 1, the tensile stress increases linearly with the tensile strain, i.e. the SWCNTs deform elastically. However, at a tensile strain of around 10%, the hexagonal cells all extend in the axial direction of the nanotubes, and that they do not return to their original geometries when the forces applied at either end of the structure are removed. This indicates that the nanotubes enter the plastic deformation regime (Stage 2). In Stage 3, the stress increases rapidly with increasing strain toward a peak value, corresponding to the maximum tensile strength (σ_{ts}) of the nanotube. When the strain is increased further, the C-C bonds in the nanotube fail, prompting the separation of the nanotube into two parts

(Stage 4). From an inspection of the linear region of the stress-strain curves computed at a temperature of T = 0.01K, the Young's modulus (E_y) of the zigzag (10,0) SWCNT is determined to be 1.21 TPa when computed using the MS data, and 1.06 TPa when computed using the MD model. Moreover, it is observed that at a temperature of 0.01 K, a good agreement exists between the stress-strain profiles predicted by the two simulation methods in both the elastic and the plastic deformation regimes. From inspection, the difference in the values of σ_{ts} predicted by the two methods is found to be less than 5%. However, a notable difference is observed in the two sets of results at strains higher than that associated with the maximum mechanical strength. Specifically, the stress predicted by the MS method falls to a value close to 0 GPa with virtually no further increase in the applied strain, whereas the stress predicted by the MD method reduces toward 0 GPa at a comparatively slower rate. It is thought that this discrepancy arises because the MS model computes the relaxed atomic structure of the nanotube solely on the basis of an energy minimization constraint, and therefore ignores the respective effects of bond rotation and competitive formations between the C-C bonds [43-44]. The Young's modulus computed using the MD model at a temperature of 300 K is found to have a value of 0.92 TPa, and is therefore lower than that computed using either the MS model or the MD model at a temperature of 0.01 K, i.e. 1.21 TPa and 1.06 TPa, respectively. This result is to be expected since materials generally have a higher stiffness at lower temperatures. Moreover, the result is consistent with that presented for SWCNTs under tension by Jeng *et al*. [45] and Shi *et al*. [46]. Overall, it is observed that the MS stress-strain curve is smoother than the two MD curves. This can be attributed to the fact that the thermally-activated fluctuations in the atom positions in the SWCNT are taken into account in the MD simulations [47-48], but are ignored in the MS model since an assumption is made that the atoms simply oscillate around their minimum-energy positions. A similar technique has also been successfully utilized to investigate into the nanoindentation size effects and mechanical contact behaviors of single asperities by *Jeng et al.* [49].

Fig. 8(b) presents the atomic configurations of the (10,0) zigzag SWCNT under the tensile strains corresponding to labels (i)–(iii) in Fig. 8(a). In the upper snapshot, produced using the MS model, it is observed that the C-C bonds in the fracture region of the nanotube are extended in the axial direction and prevent the separation of the nanotube into two parts. However, when the strain is increased beyond that associated with the maximum mechanical strength of the nanotube, these C-C bonds fracture, and thus the stress within the tube reduces virtually instantaneously to zero (see Fig. 8(a)). The middle snapshot, produced using the MD model, is broadly similar to that produced by the MS model. However, a notably greater degree of atomic structural disorder is observed in the MD results due to the inclusion of C-C bond rotation and competitive formation effects in the simulation procedure. The lower snapshot, also produced using the MD model, shows that thermal effects and over-binding mechanisms have a significant effect upon the structural deformation behavior of the zigzag (10,0) SWCNT in the higher temperature regime. Specifically, it is observed that the higher temperature deformation conditions induce a necking effect in the nanotube and prompt the formation of a small number of one-atom chains in the fracture region of the tube. As the strain is increased, these chains are extended slightly in the axial direction before breaking and thus, as shown in Fig. 8(a), the stress within the nanotube falls more slowly toward zero than that in the low-temperature tube in which no atomic chains are formed (see snapshot (ii) in Fig. 8(b)). Consequently, the present results indicate that the structural deformations of the SWCNTs are sensitive to temperature conditions. Note that these observations are consistent with the findings presented by Yakobson *et al*. [50]. The loading rate in MD simulations is much higher than that applied in practical experiments, and thus the effects of deformation-induced thermal fluctuations in the atomic configuration are overstated compared to those observed in the experimental case. However, the MS simulation model excludes the effects of the deformation-induced temperature rise and calculates the relaxed atomic configuration solely on the basis of the potential energy within the system. In other words, the MS

method is insensitive to the effects of thermal instability and kinetic excitation [51], and can therefore be reasonably expected to provide an accurate representation of the low strain rate deformation of SWCNTs. Furthermore, as commented previously, an excellent agreement exists between the MS and MD stress–strain curves in both the elastic and the plastic deformation regimes (see Fig. 8(b)), and thus the MS approach provides a valid, computationally-efficient means of determining the basic mechanical properties of SWCNTs, e.g. the Young's modulus and Poisson's ratio.

Fig. 9(a) illustrates the MS simulation results obtained for the variation of the stress with the tensile strain in the (10, 0) zigzag and (6, 6) armchair SWCNTs, respectively. To clarify the changes in the stress-strain response of the two nanotubes at different values of the applied strain, Fig. 9(b) presents snapshots of the unrolled graphitic networks of the two SWCNTs at strains corresponding to labels (I)–(III) and (i)–(iii) in Fig. 9(a), respectively. Fig. 9(a) shows that for strains of less than approximately 10%, the two stress-strain curves overlap one another and are almost linear, i.e. both tubes are within the fully-elastic deformation regime. From inspection, the Young's modulus of the (10, 0) zigzag SWCNT is found to be 1.21 TPa, while that of the (6, 6) armchair SWCNT is determined to be 1.13 TPa. This result suggests that the lower bond angles in the zigzag tube (see snapshots (I) and (i) in Fig. 9(b)) are instrumental in increasing the nanotube stiffness. As the strain is increased beyond a value of 10%, a divergence is observed between the stress-strain profiles of the two nanotubes. Specifically, for a given value of the applied strain, the stress induced in the zigzag nanotube is higher than that induced in the armchair tube (see Fig. 9(a)). The snapshots presented in (II) and (ii) in Fig. 9(b) suggest that the difference in response of the two nanotubes is the result of geometric differences in the bond orientations of the two tubes. From an inspection of Fig. 9(a), it is found that the zigzag CNT has a maximum stress of around 798 GPa at a strain of 41%, while the armchair CNT has a maximum stress of approximately 883 GPa at a strain of 46%. In other words, the armchair nanotube has a higher mechanical strength and undergoes a greater elongation prior to failure than the zigzag nanotube. Note

that a similar phenomenon was reported for the yielding of SWCNTs under tension in the MD simulations performed by Zhang *et al.* [52]. As shown in Fig. 9(b), the principal bonds in the zigzag SWCNT are aligned with the tube axis, whereas those in the armchair SWCNT are inclined at an angle. As a result, the bonds in the zigzag nanotube experience a significant change in length under the effects of the applied uniaxial strain, whereas the bonds in the armchair nanotube tend to rotate initially under the effects of the applied load. Consequently, the bonds in the zigzag nanotube are more susceptible to breakage, and thus the tube fails at a lower strain than the armchair tube.

Previous theoretical investigations have shown that the mechanical properties of a SWCNT, are insensitive to the helicity of the tube under small strains [53-54]. However, at strains higher than the yield strain, many materials deform plastically as a result of a significant distortion of the bonding topology [55-56], and thus it seems reasonable to speculate that the mechanical properties of a SWCNT may no longer be insensitive to the wrapping angle. To test this supposition, Fig. 10 plots the variation of the tensile strength of various (*n*, *n*) armchair and (*n*,*m*) zigzag SWCNTs. (Note that the simulation results are obtained using the MS model.) The results clearly show that for both types of nanotube, the maximum tensile strength increases with an increasing wrapping angle. Furthermore, it can be seen that the tensile strength is relatively insensitive to the size effect in nanotubes with a smaller diameter, but reduces significantly in the tubes with a diameter greater than 6.7 nm (e.g. the (*n*,*m*) zigzag CNT. This result is consistent with the findings of Tersoff and Ruoff [57] and is most likely attributed to the sagging characteristic of the tubular walls in SWCNTs. That is, the hollow structure of SWCNTs causes the tube to experience a certain degree of radial collapse, and therefore results in a loss in mechanical strength. The severity of the collapse increases with an increasing nanotube diameter, and thus the ultimate mechanical strength of SWCNTs reduces significantly when the diameter of the nanotube exceeds a certain critical value.

In this project, we have performed a series of MD and MS simulations to investigate the mechanical properties of single-walled carbon nanotubes under a uniaxial tensile strain. The simulations focus specifically on the effects of the nanotube helicity and the nanotube diameter on the bond length, bond angle and tensile strength of zigzag and armchair SWCNTs. In this study, a good agreement is observed between the MD and MS simulation results for the stress-strain response of the SWCNTs in both the elastic and the plastic deformation regimes. The MS simulations reveal that in the plastic deformation regime, the tensile strength of the armchair and zigzag SWCNTs increases with an increasing wrapping angle. In addition, it is shown that the tensile strength reduces significantly at larger values of the nanotube diameter. Finally, it is found that the results obtained from the molecular statics method are relatively insensitive to instabilities in the atomic structure, particularly in the absence of thermal fluctuations, and are in good agreement with the predictions obtained from the molecular dynamics method.

- **Investigation into contact behavior and tribological phenomena of nano-scale interfaces**

Tabor [58] introduced the concept of “junction growth” based on the experimental finding [59-61] that implies an increase in the contact area under tangential load. Following Tabor’s seminal study, Popelar [62] analyzed the junction growth of a rigid perfectly plasticwedge in contact with a hard smooth flat, and showed that the results were in good agreement with the experimental findings [61]. The finite element predictions for junction growth obtained by Brizmer *et al.* [63] were later confirmed by the experimental evidence presented by Ovcharenko *et al.* [64].

Many researchers have demonstrated the power of MD simulations in exploring problems at the nanoscale raised by the evolution of nanotechnology. Luan and Robbins [65-66] performed MD simulations to clarify the validity of continuum contact mechanics theory at the nanoscale. Meanwhile, Jeng *et al.* [67] utilized an atomistic methodology to examine the

full range of asperity contact behaviors and showed that the results were in good agreement with those predicted by continuum theory in the elastic, elastic-plastic, and plastic regimes. Cha *et al.* [68] performed MD simulations of a single asperity contact and showed that the force-displacement relationship had a sawtooth form due to the repetitive generation and motion of partial dislocations. Despite the ubiquitous nature of adsorbed films, the literature contains very few investigations into their effects on the interfacial phenomena between two surfaces in contact. In the few studies which do exist, McFadden and Gellman [69] reported that the presence of adsorbates with a coverage greater than 1 ML yields a significant reduction in the friction coefficient. In addition, He *et al.* [70] found that the existence of small hydrocarbon molecules or adsorbates on any surface exposed to air results in a static friction effect at the macroscopic scale. Meanwhile, Chandross *et al.* [71] showed that the friction coefficient is independent of the chain length of the adsorbed layers.

Building upon the experimental results presented in the literature for junction growth [59-61, 64] and recognizing the significance of adsorbed layers in determining the interfacial properties of two contact surfaces at the nanoscale [70-71], this present study performs a series of static atomistic simulations based upon an energy minimization method to investigate the lateral junction growth of a single asperity with and without an adsorbed layer, respectively. As shown in Fig. 11, the simulation model comprises a rigid carbon plate, a deformable copper asperity, and a layer of adsorbed atoms. In analyzing the junction growth mechanism, the slip vector analysis considers the (111) slip plane of the face centered cubic copper lattice. During the simulations, fixed boundary conditions are imposed in the (1 0 0) and (0 1 0) directions, and the carbon– copper adhesion effects between the carbon plate and the copper asperity are modeled using the Morse potential [39,72]. The interatomic forces between the atoms within the adsorbed layer and others are modeled using the Lennard-Jones potential [70]. In the simulations, the rigid carbon plate is moved downward incrementally through a displacement of 0.1 Å in each step. Following each step, the energy of the entire system is

minimized using the block-diagonal Newton–Raphson method to achieve equilibrium conditions [39]. Once the carbon plate reaches a predefined level of contact interference, it is driven in the positive *x*-axis direction through a displacement of 0.1 Å in each step until gross sliding occurs. The resulting interatomic sliding effect is then visualized using a slip vector analysis technique [73].

Fig. 12 illustrates the simulation results obtained for the maximum lateral junction growth of the asperity-plate contact pair at the inception of gross sliding for various contact interferences in the range 8–35 Å. The adsorbed layer is ignored in subfigures (a) and (b), but is considered in subfigures (c) and (d). Fig. 12(a) shows a negligible lateral junction growth under a small contact interference of 8 Å. However, a notable growth occurs when the contact interference is increased to 15 Å (Fig. 12(b)). The corresponding slip vector norm plots shown in Figs. 13(a) and 13(b), respectively, reveal that the lateral junction growth observed in the nanometer regime is primarily the result of slips of the asperity atoms caused by the tangential loading. Tabor1 contended that lateral junction growth is a plastic deformation process, which is brought about in metals by dislocations [74]. Thus, the slip vectors analyses presented in Figs. 13(a) and 13(b) substantiate the hypothesis proposed by Tabor1 that the lateral junction growth is a plastic deformation process. Fig. 12(c) shows that the existence of an adsorbed layer on the asperity results in a negligible junction growth under a moderate contact interference of 15 Å. Comparing Figs. 13(a) and 13(b), it can be seen that the adsorbed layer can lessen the shearing effect exerted by the flat on the asperity atoms. However, under a large contact interference of 35 Å, the adsorbed layer is splayed out during the loading process, resulting in the lateral growth between the asperity and the flat (Fig. 12(d)). According to Bowden and Young,19 the frictional behavior of metals is largely governed by the presence of surface films and the extent to which they reduce the amount of metallic contact. The results presented in Figs. 12(c), 12(d), 13(c), and 13(d) substantiate the well known argument of Bowden and Young [75] that a lubricant film, i.e., the

nanoscopic adsorbed layer in this simulations, has beneficial tribological properties when in the condensed state.

Fig. 14 illustrates the variation in the maximum junction growth with the dimensionless normal load for the case of no adsorbed layer and with an adsorbed layer, respectively. The theoretical results obtained from Eq. 1 in Brizmer *et al.* [63] and the experimental results presented by Ovcharenko *et al.* [64] are also presented for comparison. As shown, the maximum junction growth predicted by Brizmer *et al.* [63] reduces rapidly as the normal load is increased from 1 to 50. This result is in direct contrast to our simulation results for the case of no adsorbed layer and the experimental results presented by Ovcharenko *et al.* [64], which both show that the maximum junction growth increases with an increasing normal load. Ovcharenko *et al.* [64] explained that this deviation of theoretical6 and experimental results at a small contact interference could be attributed to the surface roughness of specimens. The results presented in Figs. 12(b) and 13(b) suggest that the increasing lateral junction growth observed over this moderate contact interference range is the result of the increasing slips of the atoms within the asperity and at the shear interface with the flat. The good agreement between the present simulation results and the experimental results suggests that the atomic slip phenomenon observed at the nanoscale represents a feasible explanation for the junction growth observed experimentally at the microscale. The asperity atoms in the initial contact area are allowed to move freely in our simulations, whereas in the continuum mechanics model, they are constrained to expand radially. As a result, the simulated value of the maximum lateral junction growth is slightly higher than that predicted by Brizmer *et al.* [63] with normal load in the range of 50–100. Brizmer *et al.* [63] explained the mechanism of junction growth by the increase in interference due to tangential loading that causes new points, which initially were outside the contact area to come into contact with the flat. Our simulation shows that the junction growth mechanism at the nanoscale is mainly the slips of asperity atoms, and a similar phenomenon that new asperity atoms come into contact with the flat is also observed.

The maximum lateral junction predictions derived using the continuum mechanics model by Brizmer *et al.* [63] disregard the adsorbed layer. To enable a like-for-like comparison of the simulation results obtained in this study under the assumption of an adsorbed layer with those presented by Brizmer *et al.* [63], it is necessary to adjust the criterion used in the simulations to represent the point of initial interfacial contact. Since lateral junction growth occurs only when the adsorbed layer is splayed out (Fig. 12(d)), we evaluate the variation in the maximum junction growth with the normal load for the case where the initial point of contact between the flat and the asperity was taken as the point at which the adsorbed layer was first fully splayed out. The corresponding results are indicated by the solid triangles in Fig. 14. It is observed that for a dimensionless normal load greater than approximately 80, a good agreement exists between the calibrated simulation results and the theoretical results derived using the continuum mechanics model.6 However, at lower values of the normal load, a noticeable deviation between the two sets of results occurs. Ovcharenko *et al.* [64] explained that this could be due to the effects of surface roughness. By contrast, a far better agreement is noted between the calibrated simulation results and the experimental data presented by Ovcharenko *et al.* [64]. This result is to be expected since both sets of results reflect the effects of an adsorbed layer on the surface of the contact asperities.

According to continuum mechanics theory, the metallic junctions formed between the contact asperities on two opposing surfaces increase in size until gross sliding occurs. Our atomistic simulations reveal that the onset of lateral junction growth is caused by the slips of the asperity atoms. Furthermore, it is shown that the presence of an adsorbed layer on the asperity surface delays the onset of lateral junction growth. The present simulation results are found to be consistent with the experimental results presented in the literature and provide a valuable interpretation of the lateral junction growth phenomenon from a nanoscale perspective.

- **Contaminant effects on the interfacial adhesion of the spatulae of a gecko: A Perspective from contact mechanics**

Many researchers have reported that the robust adhesion that enables geckos to move quickly and securely across a range of vertical and horizontal surfaces is provided by the hierarchical structure of their feet (i.e. lamellae, setae, spatulae, etc.). Maintaining this robust adhesion requires an intimate contact between the terminal tips of the spatulae and the surface. The aim of this study was to investigate the effect on the adhesive properties of the spatulae when a particle becomes trapped at the contact surface. Using the Johnson, Kendall and Roberts (JKR) theory [76], a model was constructed to assist in the analysis of the interactions between the spatula tip, the particle and the surface. Fig. 15 presents a schematic illustration of the current contact mechanics model. The model comprises three spheres with radii of R_1, R_2 and R_3, respectively, corresponding to the spatula, the particle and the surface, respectively. Note that the radius of the sphere (R_3) is signifi cantly larger than that of the spatula (R_1). Therefore, it is considered to be infi nitely large, and assumed to have the form of a fl at surface. The three spheres were brought into contact with one another via the application of an external load (P_0). Our model attempted to simplify the complex relationship between the three bodies by using a two-step approach to deal with contact properties between spatula–particle, particle–surface and spatula– surface contact pairs. The first step was to check whether the spatula covers the particle and contacts the underlying surface. The next step focused on the interactive relationship between the spatula–particle and spatula–surface contact pairs in an attempt to estimate the adhesion of the gecko-like spatula system involving a trapped particle. In macrocontact problems, the relative infl uence of adhesion is very small and can be ignored. However, in the current contact mechanics model, the characteristic sizes of the spatula and the particle are very small, and the applied load is very low. Thus, adhesive effects have a signifi cant influence on the overall behaviour of the contact system, and the work of adhesion must therefore be taken into account. Physically, the work of adhesion can be regarded as the change of surface free energy required to

separate the unit areas of two surfaces in contact with one another to a distance of infinity in a vacuum. According to JKR theory, the energy balance concept can be applied to compute the adhesion between two solids. Here, we adopted JKR theory as the basic theorem to develop the relation underlying the current contact problem with adhesive effect.

Fig. 16 illustrates the effect of the particle size on the actual contact area (a^*) for the current spatula materials of keratin and polyester examined herein. Here, the effective contact area is computed as the actual contact area normalized by the apparent contact area, i.e. $a^* = (A_{13}–A_{23}/A_{13})$. The results show that, regardless of the material of spatula, the effective contact area (a^*) varies inversely with the particle size. Furthermore, it is apparent that keratin attains a higher effective contact area than that recorded for polyester, regardless of the particle size. Again, this result is attributed to the lower work of adhesion of polyester compared with keratin. Fig. 17 clearly shows that keratin results in a far higher adhesion than does polyester, particularly at higher values of the applied load. Furthermore, Fig. 18 shows that a keratin spatula (of width approximately 200 nm) is capable of maintaining an effective contact area for particle of up to 32 nm ($A_{23}\approx A_{13}/5$) for applied loads lower than 300 nN.

Fig. 19 illustrates the relationship between the adhesion and the applied load for the case of concrete, glass, wood and SiO_2 surfaces. For the hard surfaces (i.e. SiO2 and glass), it is observed that the magnitude of the applied load has little effect on adhesion. For these surfaces, the particle is unable to intrude into the hard surface to any great depth, and hence the contact area between the particle and the surface (A_{23}) is small. Under these conditions, A_{23} approaches 0, and the size of the actual contact area is dominated by the spatula. The adhesion of the spatula to the surface is constant because, according to JKR theory, its value is given by $–3/2\pi W_{13}R_{13}$, in which W_{13} both R_{13} and are constant. However, for softer surfaces, i.e. concrete and wood, Fig. 19 shows that the adhesion increases with increasing load. The adhesion is significantly larger than that achieved on a hard surface, particularly under

higher values of the applied load, due to the higher contact interface of the soft surface.

In this study, we have explored the contact relationships of nano-structural gecko setae. For macro-contact systems, tiny particles can be ignored because their scale is small compared to that of the contact body. On the contrary, particles cannot be disregarded for systems relying upon the nano-contact system. The current study reported on numerical simulations based on a contact mechanics model and JKR theory to explore the effect of trapped particles on the adhesive capabilities of the spatulae of gecko setae in relation to substrates of various types. Our results showed that the keratin (the natural material of the spatula) provides a robust system for adhesion even when there is a particle in the contact area, and the effective contact area of spatulae will be 80%. When the particle is signifi cantly harder than the surface, the adhesion properties of the contact surface infl uenced by the particle will be more obvious. The results also reveal that the generated adhesion is considerably higher when the spatula is in contact with a softer surface, such as wood or concrete, rather than a hard surface, such as glass or SiO_2.

Summary

The present program is an integrated project to conduct concerted team effort for the quantification of nano-material systems. Nano-mechanisms for material strength, tribological performances and contact behavior between two solid surfaces have been investigated. In this project, coupling of atomistic and continuum simulations provides a computationally efficient mechanism for investigating not only the interfacial behavior at a fundamental nano-scale, but also other scale, including meso-scale, micro-scale and multi-scale.

This project has presented static atomistic simulations of the previously unexplored question of how nanoindentation is influenced by the presence of a void. Our simulation reveals that the void disappears when the indentation

depth is sufficiently large. A stress concentration is observed at the internal surface of the void in all simulations cases. Meanwhile, observation of the dislocation structure by means of slip vector analysis has shown that deformation in nanoindentation is not influenced significantly by the presence of a void. The results indicate that the presence of a void has a significant influence on the nanohardness extracted from the nanoindentation tests. Molecular dynamic simulations have also been employed to demonstrate that the effect of indentation velocities has a direct influence on *c*-Si during nanoindentation processes. An amorphization has also been confirmed from load dependent indentation where increased amount of amorphized phase is made responsible for the increasing elastic recovery of the sample with increasing load. Furthermore, we also employ a series of molecular dynamics (MD) and molecular statics (MS) simulations to investigate the mechanical properties of carbon nanotubes under a uniaxial tension. The simulations focus specifically on the effects of the nanotube helicity and the nanotube diameter on the bond length, bond angle and tensile strength of zigzag and armchair SWCNTs. In this study, a good agreement is observed between the MD and MS simulation results for the stress-strain response of the SWCNTs in both the elastic and the plastic deformation regimes. The MS simulations reveal that in the plastic deformation regime, the tensile strength of the armchair and zigzag SWCNTs increases with an increasing wrapping angle. In addition, it is shown that the tensile strength reduces significantly at larger values of the nanotube diameter. Moreover, it is observed that the tensile strength of both SWCNTs reduces as the percentage of defects within the nanotube structure increases. Finally, it is found that the results obtained from the molecular statics method are relatively insensitive to instabilities in the atomic structure, particularly in the absence of thermal fluctuations, and are in good agreement with the predictions obtained from the molecular dynamics method. This project has also performed that the onset of lateral junction growth in the nanometer regime is primarily the result of the slips of atoms

within the asperity, which causes new asperity atoms come into contact with the flat. Since the plastic deformation of crystalline solids is known to be the result of dislocations, our simulation results substantiate that the assertion of junction growth is essentially a plastic deformation process. Moreover, the simulation results reveal that the presence of an adsorbed layer on the asperity surface significantly delays the onset of lateral junction growth until the adsorbed layer is splayed out from the interface. Our simulation results provide a useful elucidation of the lateral junction growth phenomenon observed at the micro-scale. Moreover, our study has investigated into the effect on the adhesive properties of the spatulae when a particle becomes trapped at the contact surface. Using the Johnson, Kendall and Roberts (JKR) theory, a model was constructed to assist in the analysis of the interactions between the spatula tip, the particle and the surface. The results showed that the keratin (the natural material of the spatula) provides a robust system for adhesion even when there is a particle in the contact area, and the effective contact area of spatulae will be 80%. When the particle is significantly harder than the surface, the adhesion properties of the contact surface influenced by the particle will be more obvious. The results also reveal that the generated adhesion is considerably higher when the spatula is in contact with a softer surface, such as wood or concrete, rather than a hard surface.

Ultimately, we have developed a systematic approach to gain a valuable insight of the interfacial behavior for both the modeling community and those in industry wanting to know more about how multi-scale materials modeling can help optimal product and process design.

References

[1] E. M. Bringa *et al.*, *Science* **309**, 1838 (2005)

[2] V. Gavini, Phys. Rev. Lett. **101**, 205503 (2008)

[3] X. L. Wu and Y. T. Zhu, Phys. Rev. Lett. **101**, 025503 (2008)

[4] D. M. Mitnik *et al.* Phys. Rev. A **78**, 062501 (2008)

[5] J. Karch *et al.*, Nature **330**, 556 (1987)

[6] Y. D. Wang *et al.*, Nature Mater. **2**, 101 (2003)

[7] M. I. Elhaj and M. Schadt, Nature **410**, 796 (2001)

[8] M. Urbakh *et al.*, Nature **430**, 525 (2004)

[9] A. Carpinteri and N. Pugno, Nature Mater. **4**, 421 (2005)

[10] B. Bhushan and M. Nosonovsky, Acta Mater. **52**, 2461 (2004)

[11] E.O. Hall, *Proceedings of the Physical Society of London,* **64,** 747 (1951)

[12] N. J. Petch, J. Iron and Steel Inst. **174**, 25 (1953)

[13] G. I. Taylor, J. Institute Metals **62**, 307 (1938)

[14] S. R. Kalidindi *et al.*, J. Mech. Phys. Solids **40**, 537 (1992)

[15] P. Van Houtte *et al.*, Inter. J Plast. **21**, 589 (2005)

[16] J. Schiøtz *et al.*, Nature **391**, 561 (1998)

[17] H. Van Swygenhoven, Science **296**, 66 (2002)

[18] Y. R. Jeng and C. M. Tan, Appl. Phys. Lett. **89**, 1 (2006)

[19] A. Latapie and D. Farkas, Scripta Mater. **48**, 611 (2003)

[20] J. Y. Shu, Int. J. Plasticity **14**, 1085 (1998)

[21] L. Farrissey *et al.*, Comput. Mater. Sci. **18**, 102 (2000)

[22] L. Kogut and I. Etsion, Trans. ASME, J. Appl. Mech. **69**, 657 (2002)

[23] R. L. Jackson and I. Green, ASME J. Tribol. **127**, 343 (2005)

[24] B. Luan and M. O. Robbins, Nature **435**, 929 (2005)

[25] P. R. Cha *et al.*, Acta Materialia **52**, 3983 (2004)

[26] J. Tersoff, Phys. Rev. Lett. **61**, 2879 (1988)

[27] J. Tersoff, Phys. Rev. B **37**, 2879 (1988)

[28] J. Tersoff, Phys. Rev. B **39**, 5566 (1989)

[29] W. Lu and K.J. Komvopoulos, ASME J. Tribol. **123**, 641 (2001)

[30] J.A. Zimmerman *et al.*, Phys. Rev. Lett. **88**, 36101 (2002)

[31] J.A. Zimmerman *et al.*, Phys. Rev. Lett. **87**, 165507 (2001)

[32] E.T. Lilleodden *et al.*, J. Mech. Phys. Sol. **51**, 901 (2003)

[33] J. Knap and M. Ortiz, Phys. Rev. Lett. **90**, 226102 (2003)

[34] S. Iijima, Nature **21**, 56 (1991)

[35] D. S. Bethune *et al.*, Nature **363**, 605 (1993)

[36] T. W. Ebbesen and P. M. Ajayan, Nature **358**, 220 (1992)

[37] J. Qiu *et al.*, Carbon **41**, 2170 (2003)

[38] A. Thess, *et al.*, Science **273**, 483 (1996)

[39] Y. R. Jeng and C. M. Tan, Phys. Rev. B **65**, 174107 (2002)

[40] C. L. Liu, and S. J. Plimpton, Phys. Rev. B **51**, 4523 (1995)

[41] Y. R. Jeng and C. M. Tan, Phys. Rev. B **69**, 104109 (2004)

[42] Y. R. Jeng and C. M. Tan, ASME J. Tribol. **126**, 767

[43] B.I. Yakobson *et al.*, Phys. Rev. Lett. **81**, 4656 (1998)

[44] D. Orlikowski *et al.*, Phys. Rev. Lett. **83**, 4132 (1999)

[45] Y. R. Jeng *et al.*, J. Phys. Chem. Sol. **65**, 1849 (2004)

[46] S. Q. Shi and L. G. Zhou, Comp. Mater. Sci. **23**, 166 (2002)

[47] G. Q. Xie and S. Y. Long, Comput., Mater. & Continua **4**, 11 (2006)

[48] G. Q. Xie and S. Y. Long, Comput., Mater. & Continua **6**, 1 (2007)

[49] Y. R. Jeng *et al.*, Appl. Phys. Lett.,**91**, 91904 (2007)

[50] B. I. Yakobson *et al.*, Comp. Mater. Sci. **8**, 341 (1997)

[51] W. C. D. Cheong *et al.*, Key Eng. Mater. **196**, 31 (2001)

[52] P. Zhang *et al.*, Phys. Rev. Lett. **81**, 5346 (1998)

[53] D. H. Robertson *et al.*, Phys. Rev. B **45**, 12592 (1992)

[54] J. P. Lu, Phys. Rev. Lett. **79**, 1297 (1997)

[55] T. Ozaki *et al.*, Phys. Rev. Lett. **84**, 1712 (2000)

[56] Y. R. Jeng *et al.*, J. Chem. Phys. **122**, 224713. (2004)

[57] J. Tersoff and R. S. Ruoff, Phys. Rev. Lett. **73**, 676 (1998)

[58] D. Tabor, Proc. R. Soc. London, Ser. A **251**, 378 (1959)

[59] J. S. McFarlane and D. Tabor, Proc. R. Soc. London, Ser. A **202**, 244 (1950)

[60] R. Parker and D. Hatch, Proc. Phys. Soc. London, Sect. B **63**, 185 (1950)

[61] J. S. Courtney-Pratt and E. Eisner, Proc. R. Soc. London, Ser. A **238**, 529 (1957)

[62] C. H. Popelar, ASME Trans. J. Appl. Mech. **36**, 132 (1969)

[63] Brizmer *et al.*, ASME J. Tribol. **129**, 783 (2007)

[64] Ovcharenko *et al.*, Wear **264**, 1043 (2008)

[65] B. Q. Luan and M. O. Robbins, Nature **435**, 929 (2005)

[66] B. Q. Luan and M. O. Robbins, Phys. Rev. E **74**, 026111 (2006)

[67] Jeng *et al.*, Appl. Phys. Lett. **91**, 091904 (2007)

[68] Cha *et al.*, Acta Mater. **52**, 3983 (2004)

[69] C. F. McFadden and A. J. Gellman, Surf. Sci. **409**, 171 (1998)

[70] G. He *et al.*, Science **284**, 1650 (1999)

[71] M. Chandross *et al.*, Langmuir **24**, 1240 (2008)

[72] Y. R. Jeng *et al.*, Appl. Phys. Lett. **89**, 251901 (2006)

[73] J. A. Zimmerman *et al.*, Phys. Rev. Lett. **87**, 165507 (2001)

[74] D. Hull and D. J. Bacon, *Introduction to Dislocation* (Butterworth Heinemann, Oxford, 2001)

[75] F. P. Bowden and J. E. Young, Proc. R. Soc. London, Ser. A **208**, 311 (1951)

[76] K. L. Johnson *et al.*, *Proc. R. Soc. Lond. A* **324**, 301 (1971)

Table 1 Nanohardness values for two void parameters (void size and depth)

Void parameters (size and depth)	Maximum load (10 eV/nm)	Nanohardness (Gpa)
No void	222	6.27
Size = 0.8 nm Depth = 1.3 nm	194	5.58
Size = 1.2 nm Depth = 1.0 nm	183	5.32
Size = 1.2 nm Depth = 1.5 nm	190	5.52
Size = 1.2 nm Depth = 2.0 nm	196	5.69
Size = 1.6 nm Depth = 1.7 nm	182	5.29

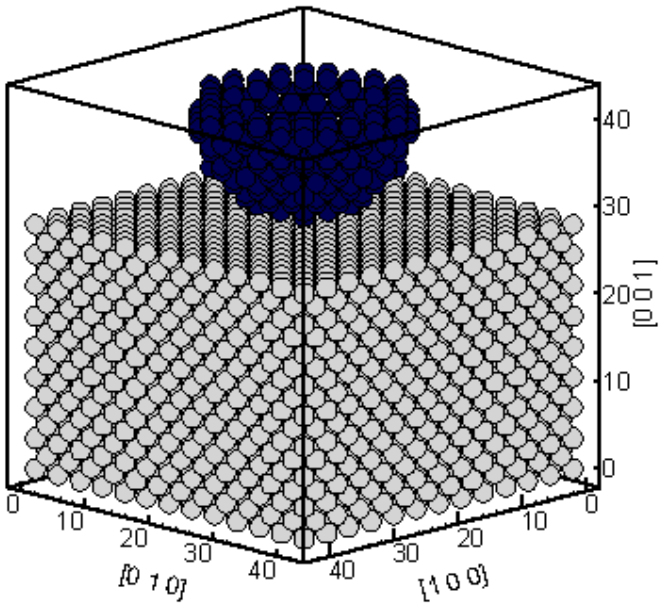

Fig. 1. Atomistic model used in nanoindentation simulations (units: Angstrom).

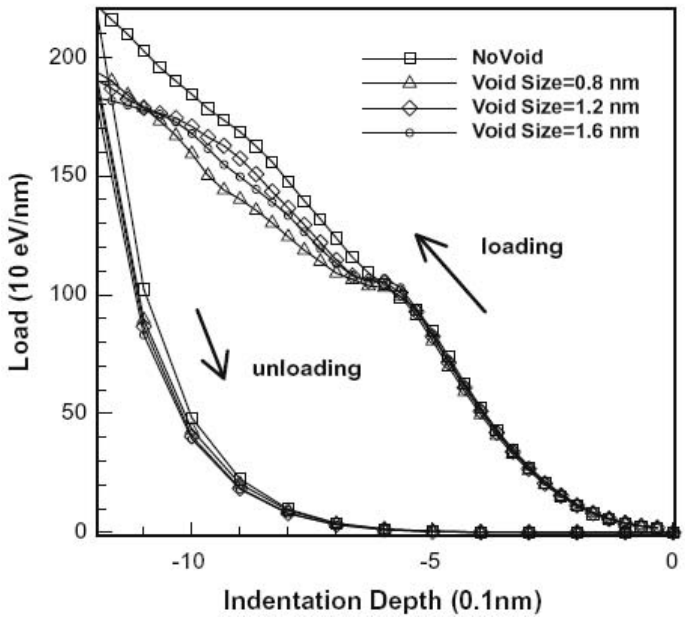

(a) variation of void size

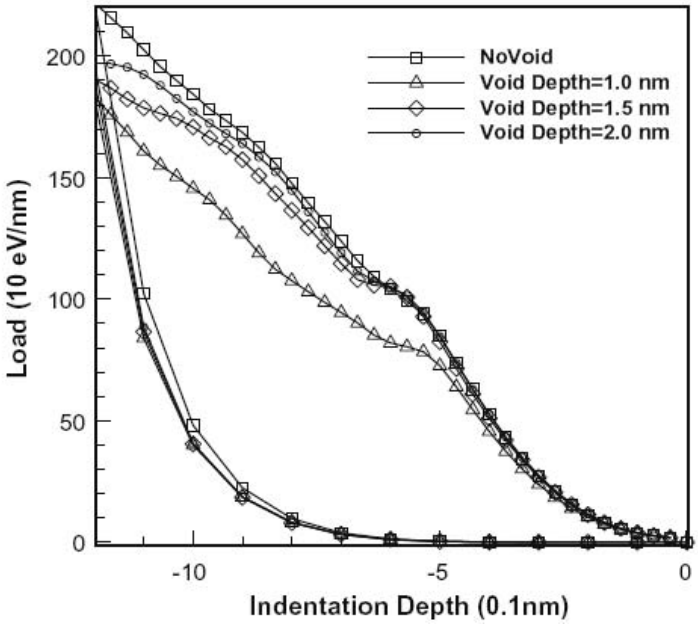

(b) variation of void depth

Fig. 2. Load-depth curves for two void parameters: (a) void size and (b) void depth.

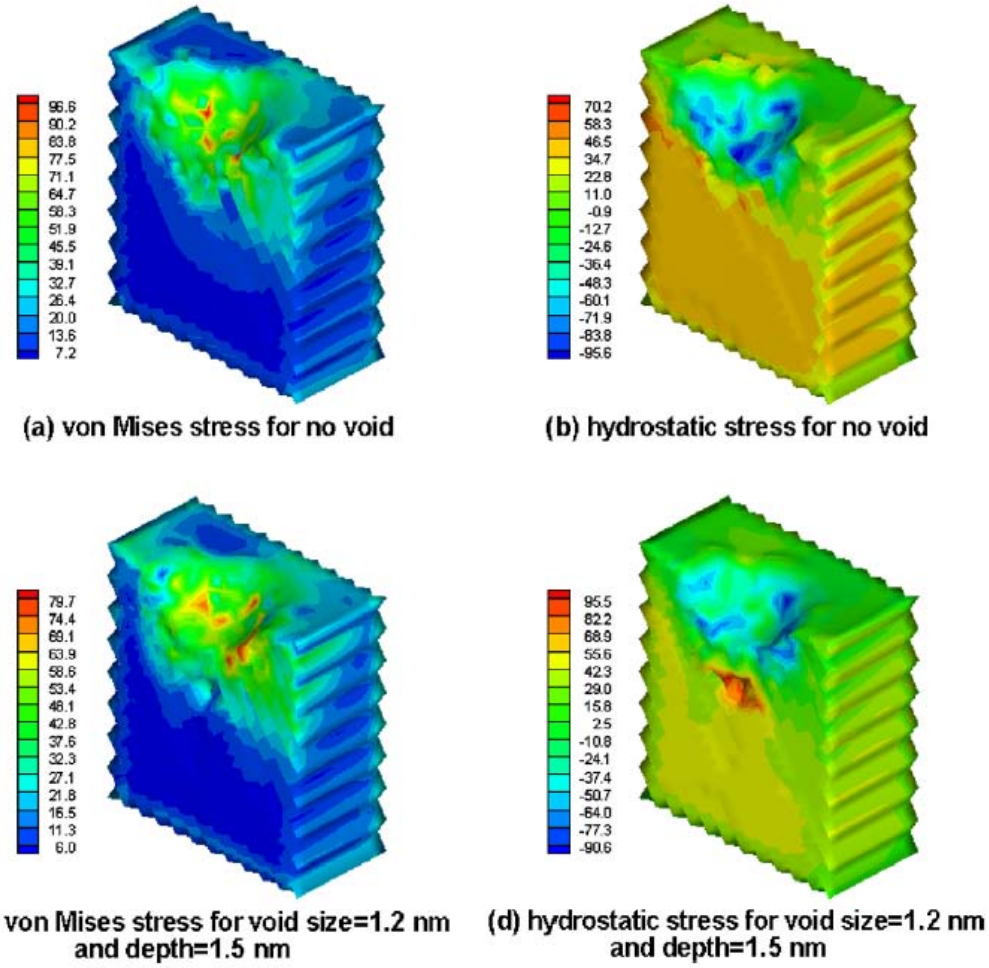

Fig. 3. Distributions of hydrostatic stress and von Mises stress in cross-section through indenter and parallel with (-101) plane: (a) von Mises stress for no void. (b) Hydrostatic stress for no void. (c) von Mises stress for void size = 1.2 nm and depth = 1.5 nm. (d) Hydrostatic stress for void size = 1.2 nm and depth = 1.5 nm (stress unit: 0.1 Gpa).

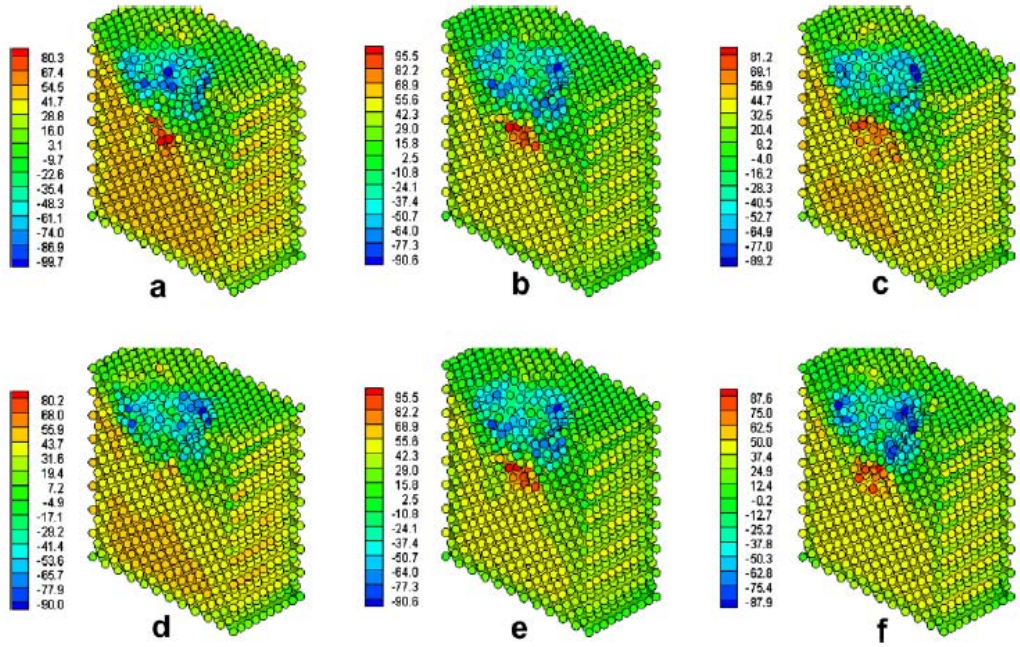

Fig. 4. Variation of hydrostatic stress distribution in cross-section through indenter tip with two void parameters: (a–c) void size = 0.8, 1.2, and 1.5 nm. (d–f) Void depth = 1.0, 1.5, and 2.0 nm.

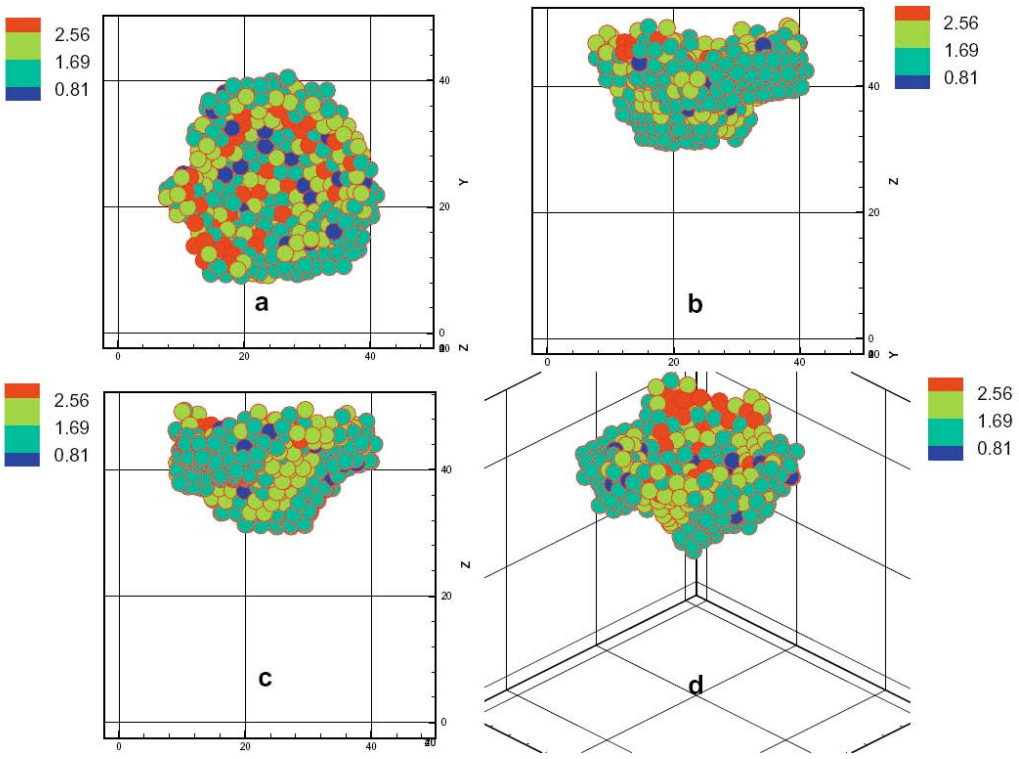

Fig. 5. Scatter subplots of distribution of slip vector norm for no void case viewed in: (a) [111], (b) [101], (c) [121], and (d) isometric directions, respectively (unit: Angstrom).

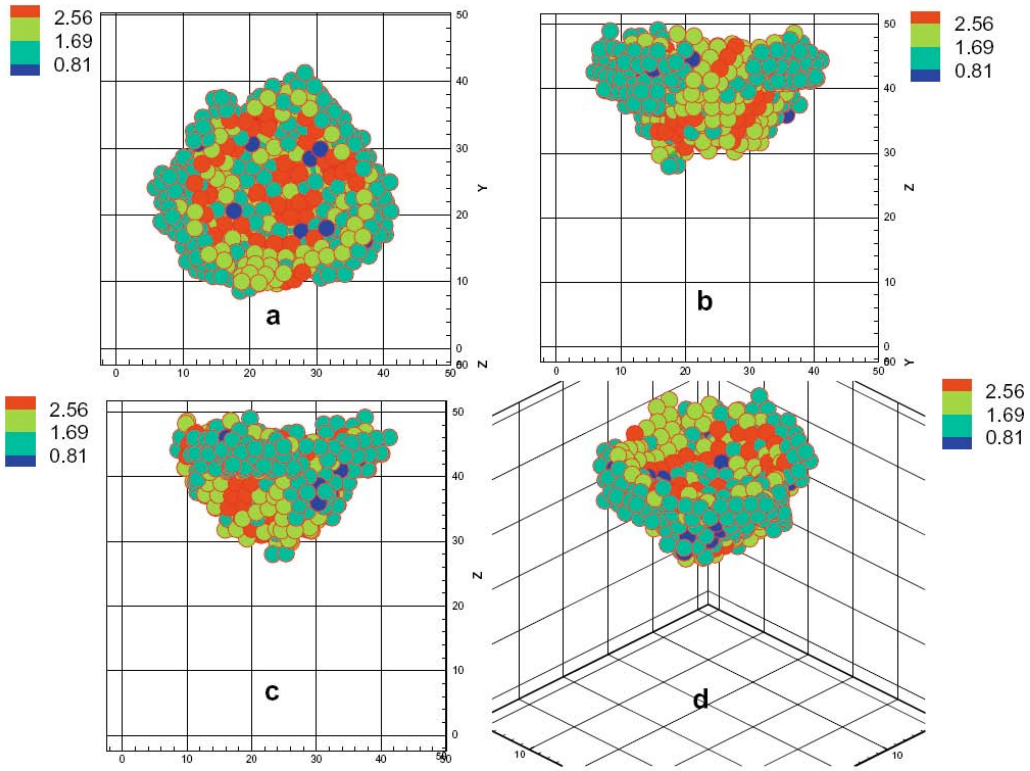

Fig. 6. Scatter subplots of distribution of slip vector norm for void size = 1.2 nm and void depth = 1.5 nm viewed in: (a) [111], (b) [101], (c) [121], and (d) isometric directions, respectively (unit: Angstrom).

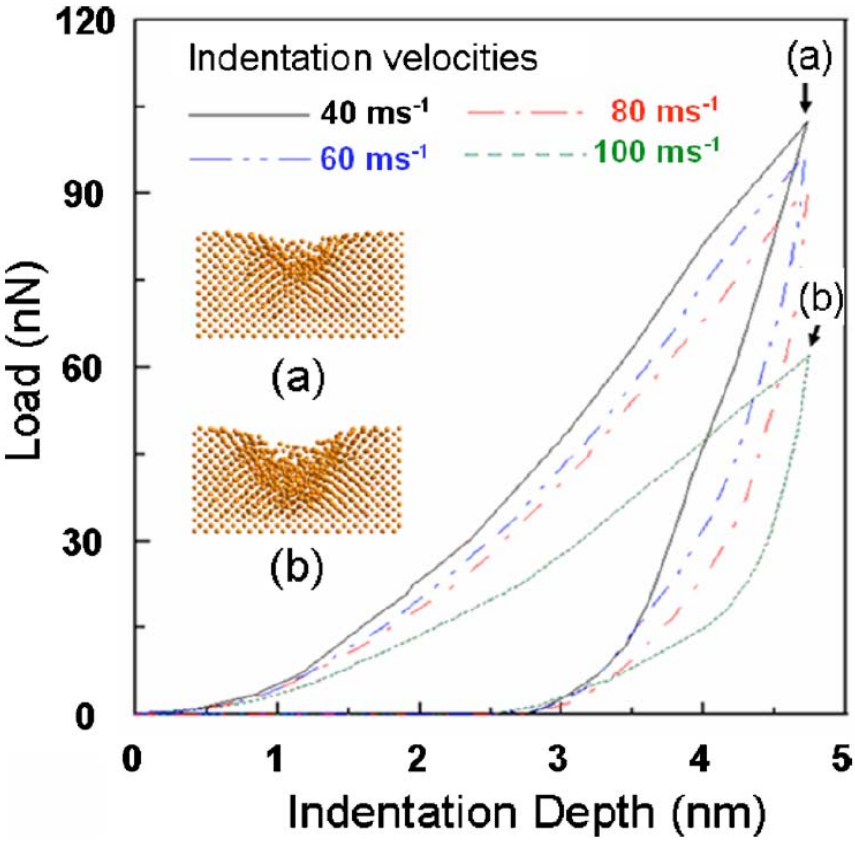

Fig. 7. Variation in force with displacement for silicon films at various indentation velocities of *V*=40, 60, 80, and 100 ms−1. Snap shots of the simulation indicating different stages of deformation (a) and (b). Corresponding load-unload curves are also indicated.

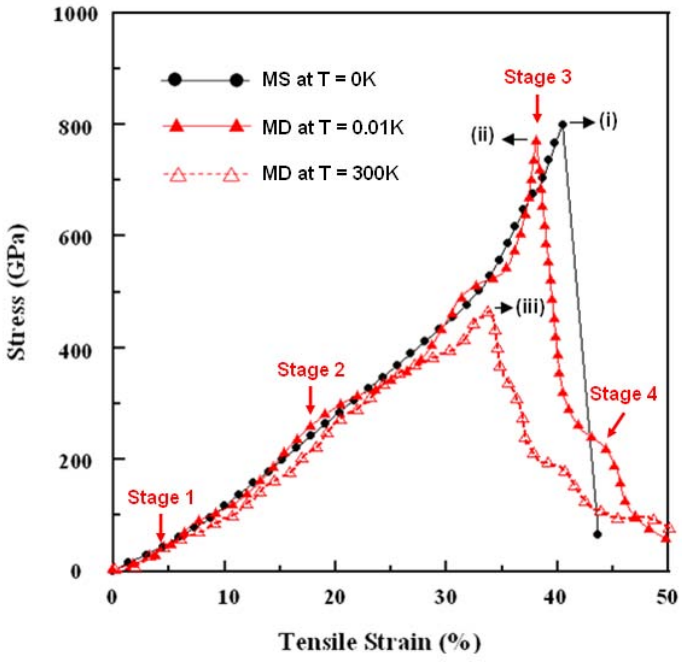

(a)

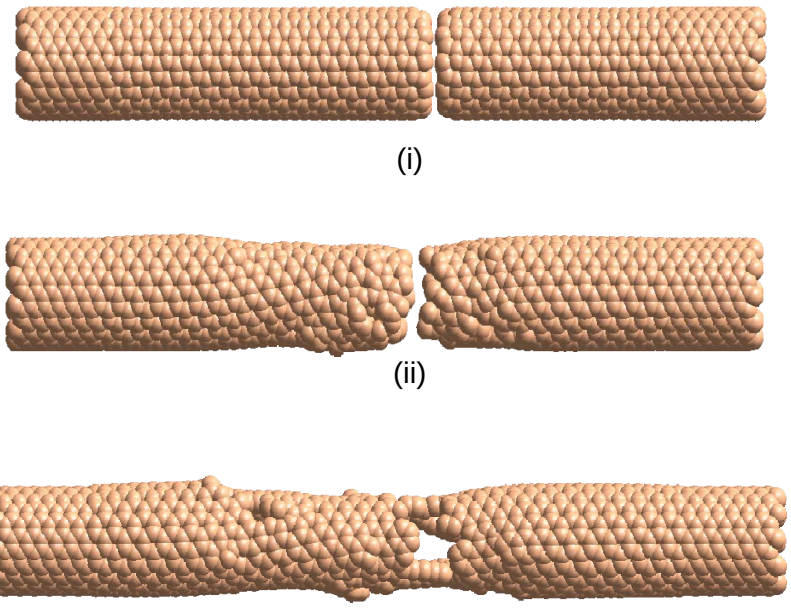

(i)

(ii)

(iii)

(b)

Fig. 8 (a) Stress–strain curves of (10, 0) zigzag SWCNT as predicted by molecular statics and molecular dynamics simulations, respectively. (b) Typical snapshots of (10, 0) zigzag SWCNT under uniaxial strains corresponding to labels (i)–(iii) in Fig. 1(a). (Note that labels (i)–(iii) indicate positions of maximum stress used to determine maximum tensile strength of nanotube.)

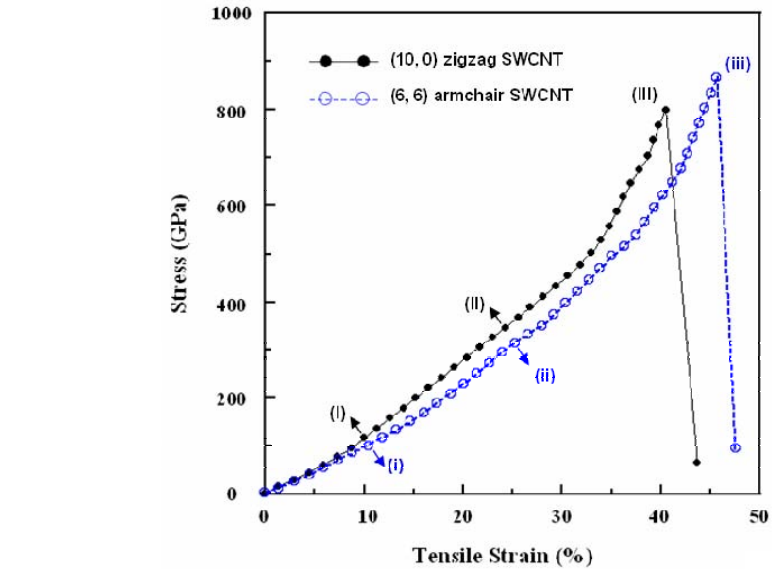

(a)

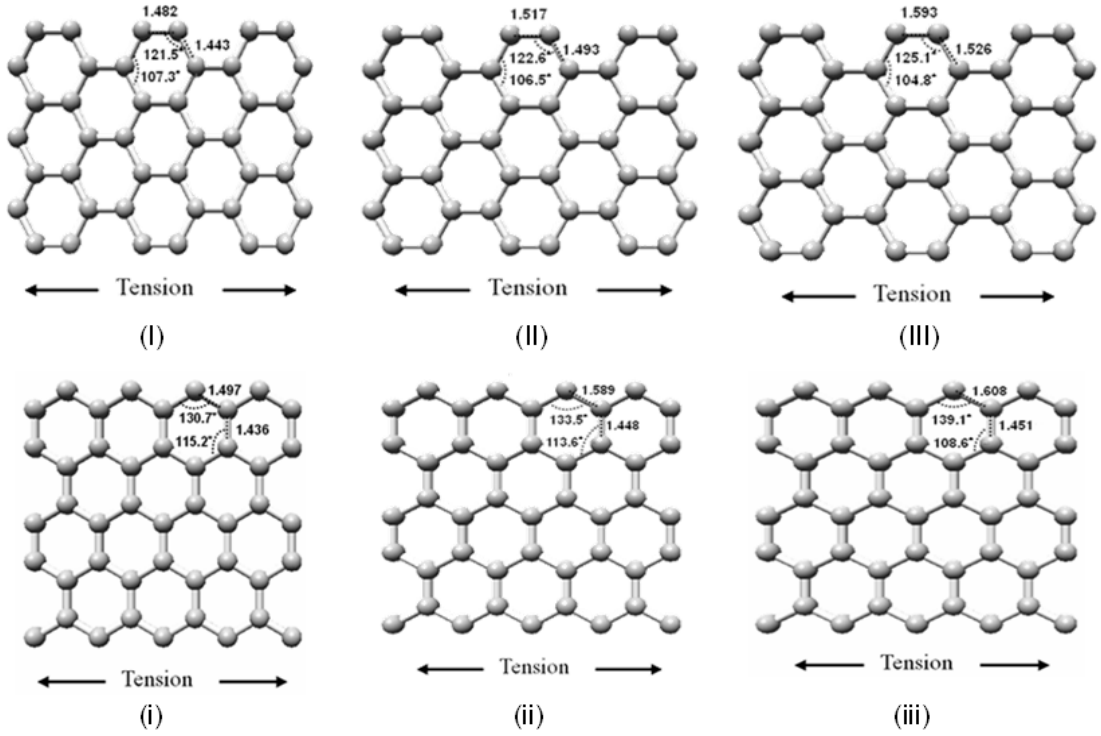

(b)

Fig. 9 (a) Variation of stress with tensile strain for zigzag (10, 0) and armchair (6, 6) SWCNTs. (Note that labels (I)–(III) and (i)–(iii) denote different deformation stages of zigzag and armchair tubes, respectively, and correspond to snapshots presented in Fig. 2(b)). (b) Structural changes in zigzag (10, 0) and armchair (6, 6) SWCNTs during tensile testing. (Note that bond length measurements are given in angstroms while bond angles are given in degrees.)

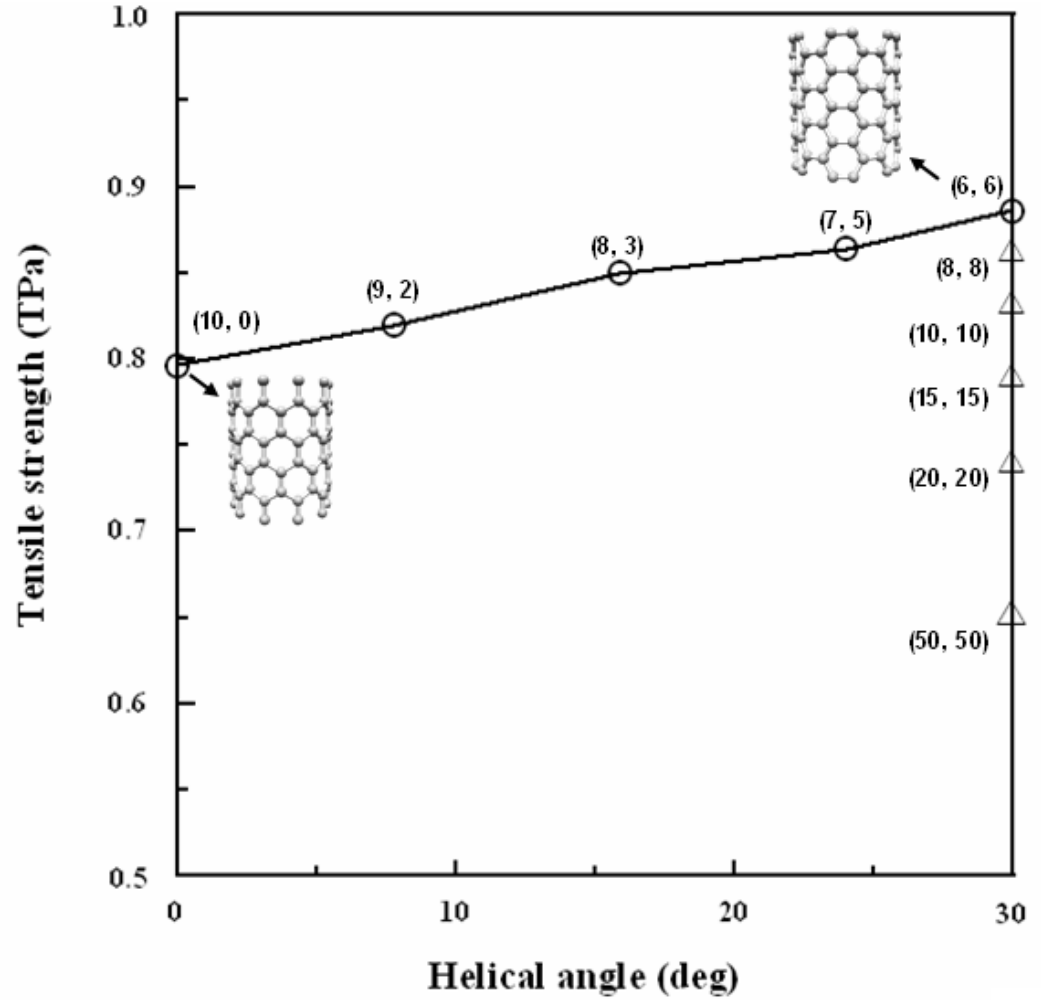

Fig. 10 Variation of tensile strength with helical angle for various (*n*, *m*) zigzag SWCNTs and (*n*, n) armchair SWCNTs.

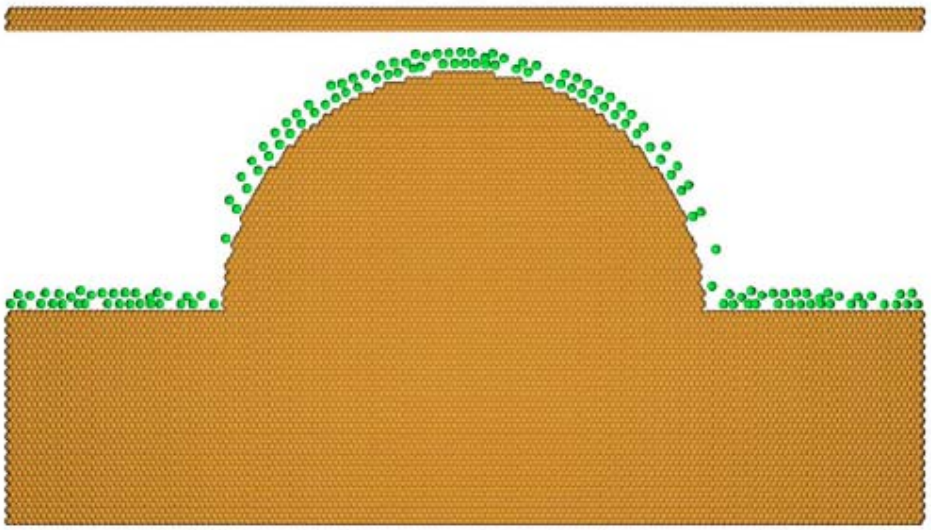

Fig. 11 An atomistic simulation model of asperity-plate contact system with adsorbed layer.

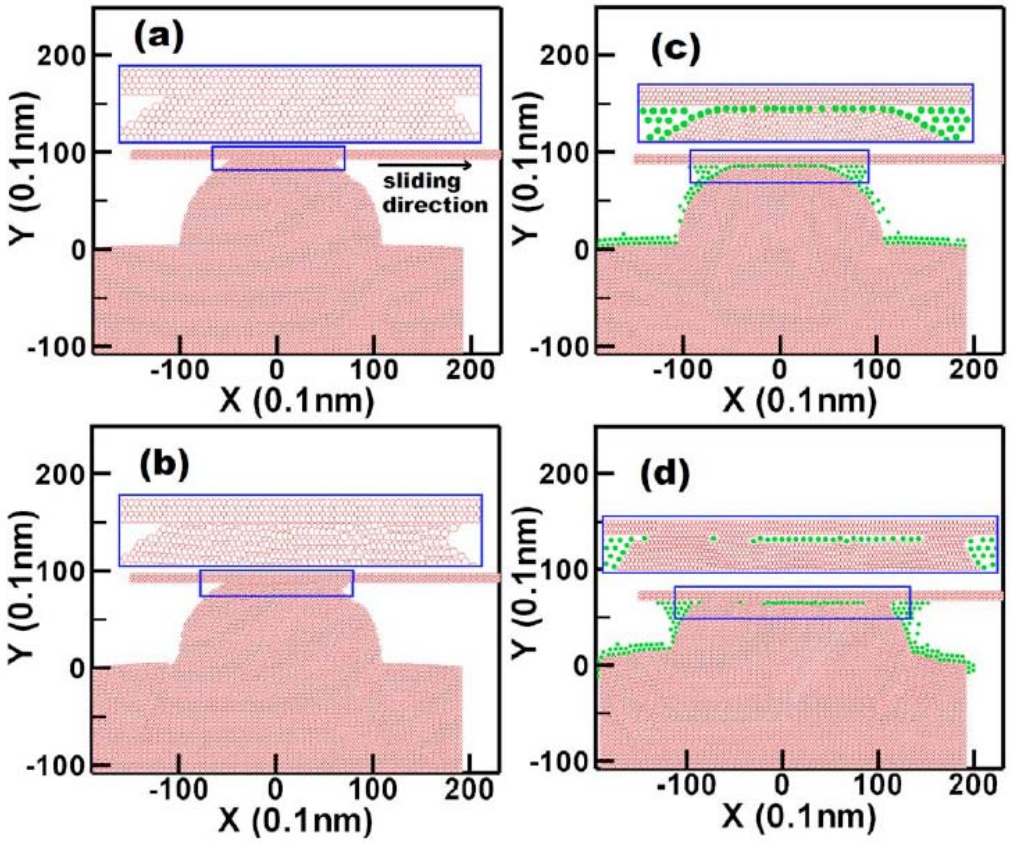

Fig. 12 Atomistic configurations of maximum lateral junction growth of contact area for initial contact interferences of (a) 8 Å, (b) 15 Å, (c) 15 Å, and (d) 35 Å. Note that [(a), (b)] and [(c), (d)] show the junction growth phenomenon without and with an adsorbed layer (shown in green), respectively.

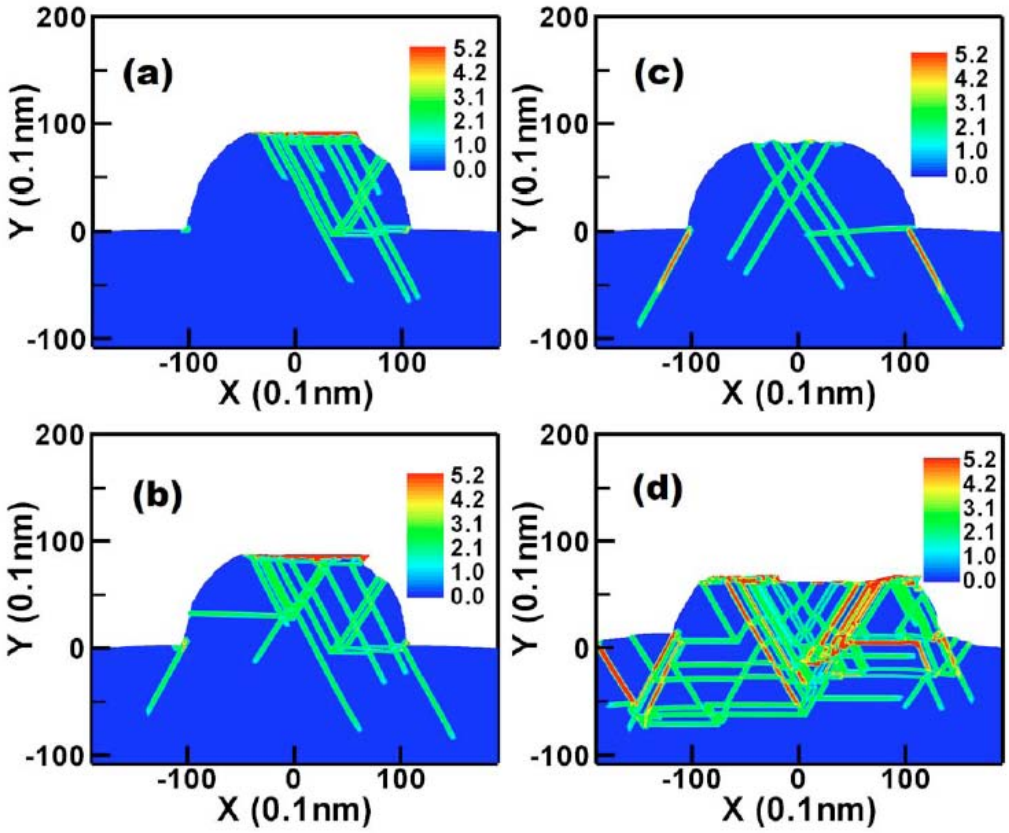

Fig. 13 Slip vector norm plots corresponding to equivalent atomistic configurations shown in Fig. 12.

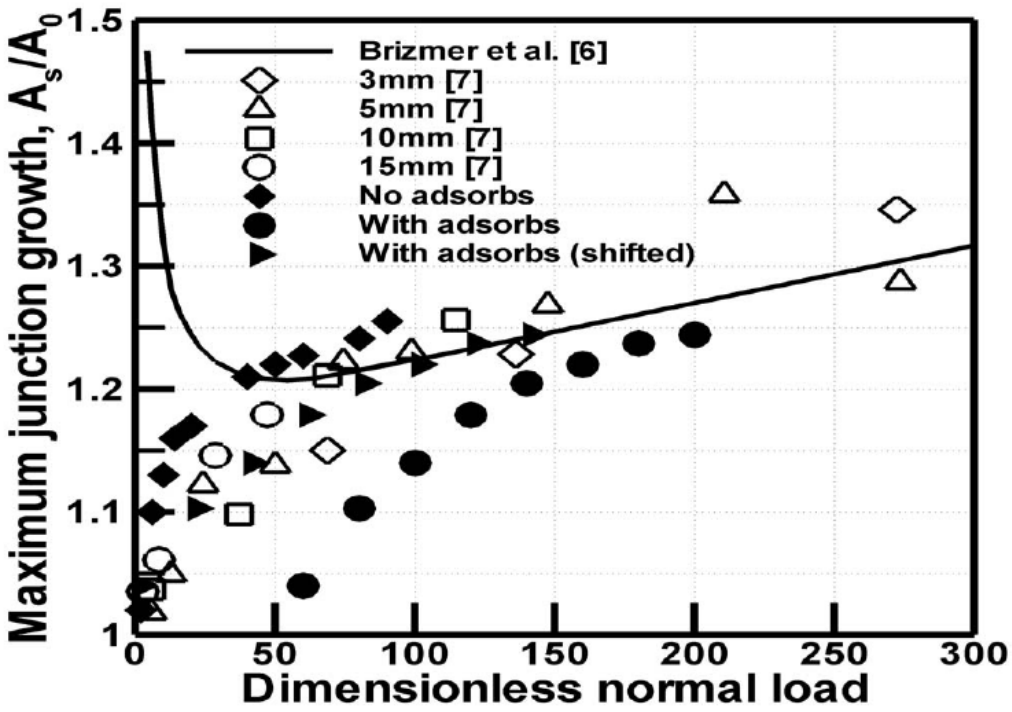

Fig. 14 Variation of maximum lateral junction growth with dimensionless normal load both with (solid circle) and without (solid diamond) adsorbed layer. [Note that for comparison purposes, the figure also shows the results derived from Eq. 1 in Ref. 63 (solid line) and the experimental results presented in Ref. 64].

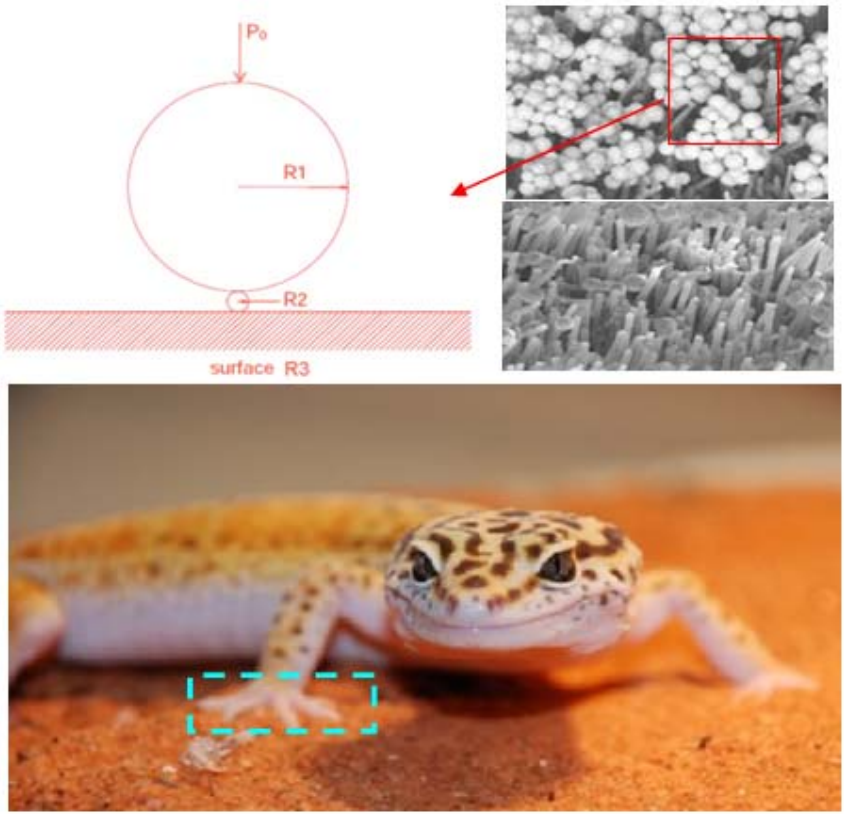

Fig. 15 The schematic illustrates the contact mechanics model that comprises three spheres with radii of *R*1, *R*2 and *R*3 corresponding to the spatula, the particle and the surface, respectively. The spatula is so tiny that the radius of *R*1 is far smaller than the radius of *R*3. Therefore, the sphere (*R*3) can be considered to be infinitely large, and assumed to have the form of a flat surface.

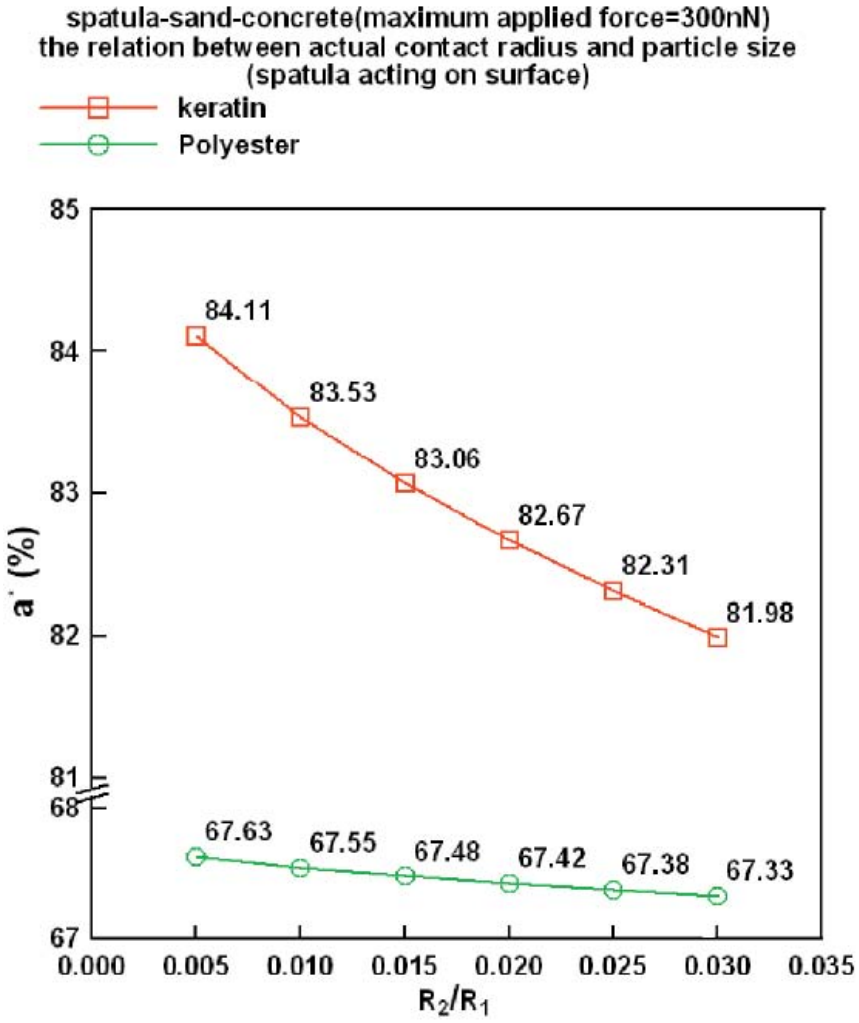

Fig. 16 The case is that two materials of spatula, i.e. keratin and polyester, contact with concrete surface, which exists the various scales of particle. Regardless of the material of spatula, the effective contact area (*a**) varies inversely with the particle size. In general, the keratin

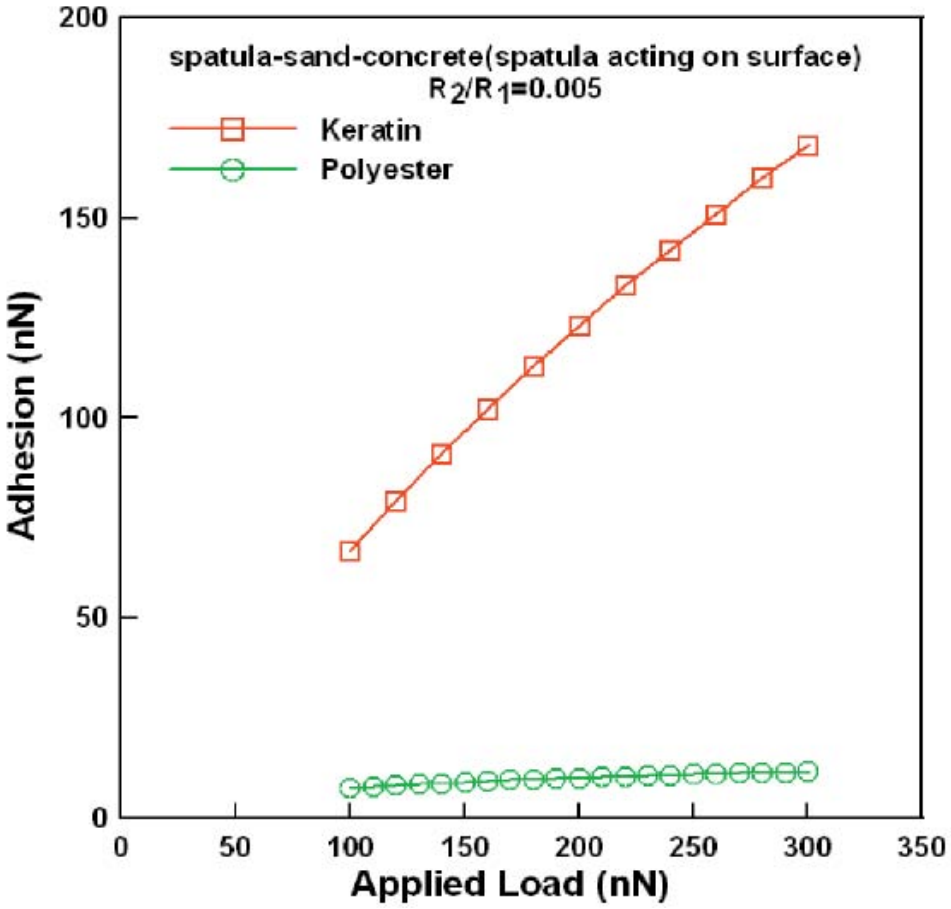

Fig. 17 For the same size of particle, the adhesions of both keratin and polyester spatula increase proporationately to add the applied load. It clearly shows that the adhesions of keratin spatula is far higher than that of polyester

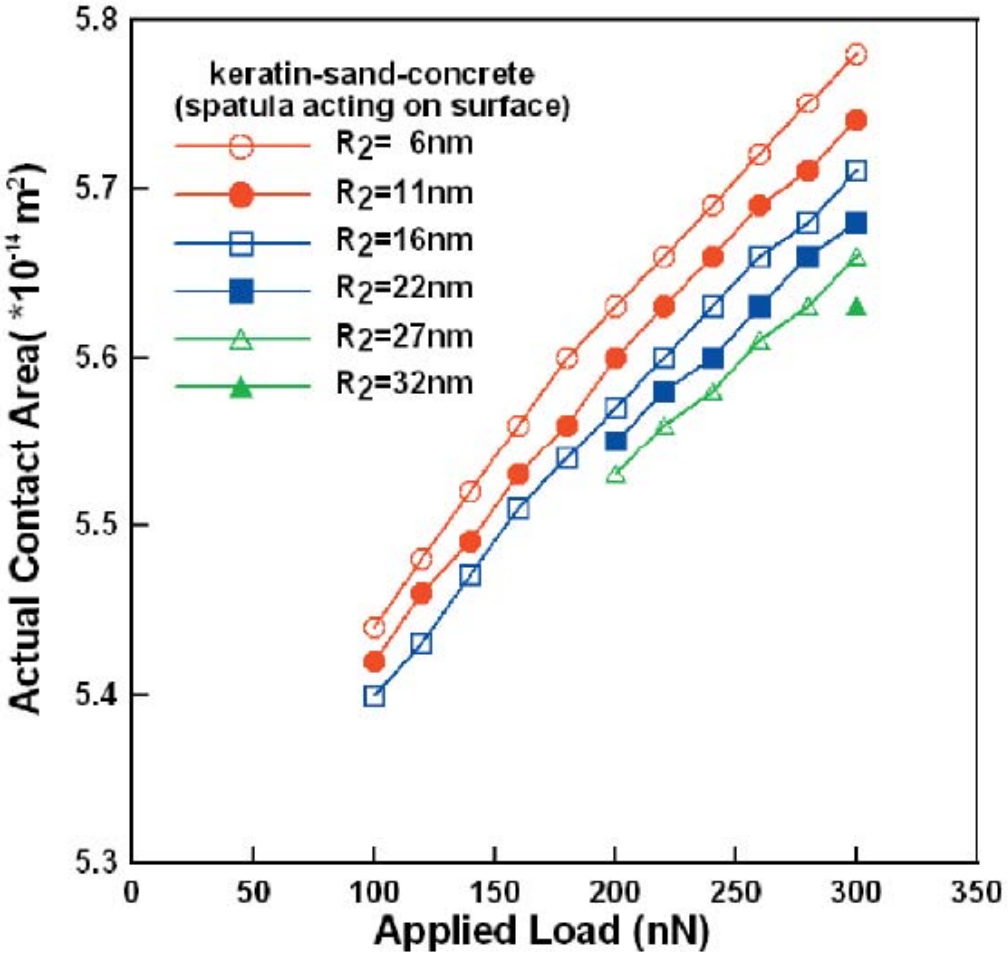

Fig. 18 When the keratin spatula contacts with concrete surface, the variation of contact area with applied load as function of radial ratio for spatula–sand–concrete contact model is shown. The keratin spatula is capable of maintaining an effective contact area for particle of up to 32 nm for applied loads lower than 300 nN.

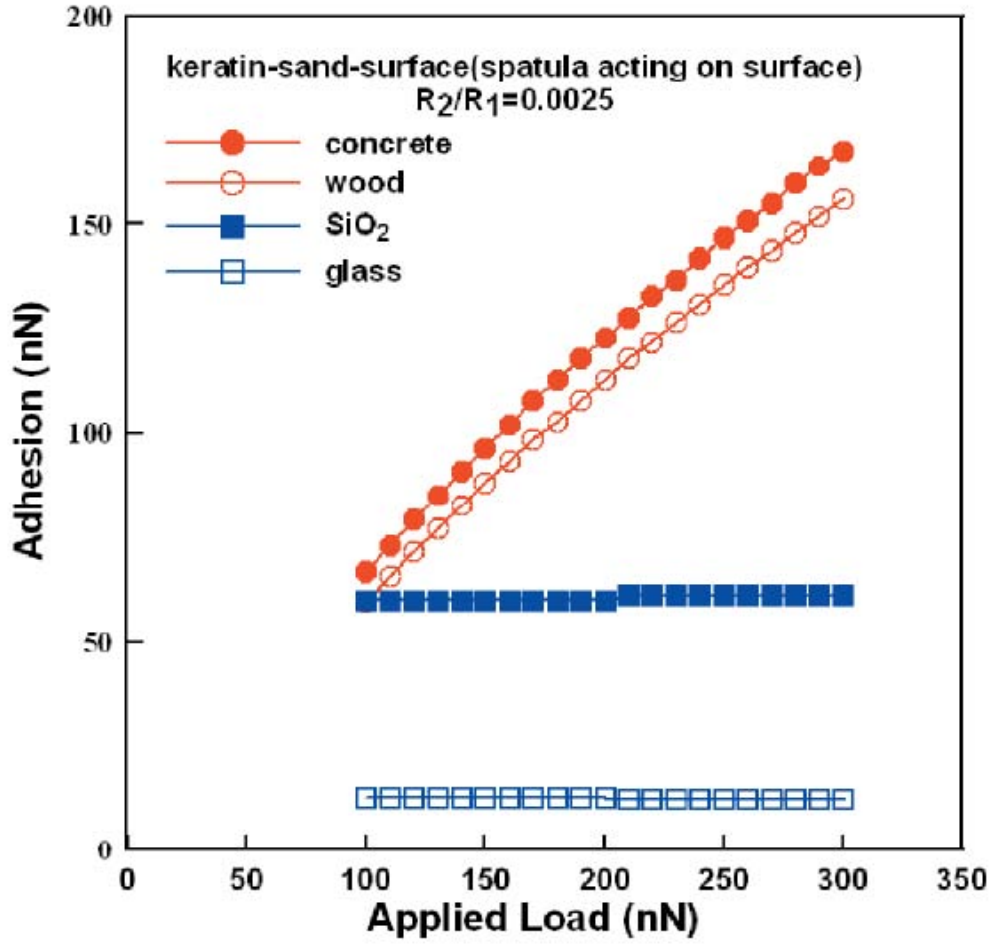

Fig. 19 Regardless of the variation of scale of the particle, the adhesions of the spatula increase proporationately to the applied load for softer surface, i.e. concrete and wood. For hard surfaces (i.e. SiO_2 and glass), it is observed that the magnitude of the applied load has little effect on the adhesion.

List of Publications

Yeau-Ren Jeng, H. C. Wen, and P. C. Tsai, 2009, “The Effect of Ni Catalytic Nanoparticle on the Growth of Carbon Nanotubes: A Perspective from Nanotribological Characterization,” Diamond & Related Materials, Vol. 18, Issue 2-3, pp. 528-532 (SCI)

C. M. Tan, and Yeau-Ren Jeng, 2009, “Computer Simulations of Nanoindentation on Cu (111) with a Void,” International Journal of Solids and Structures, Vol. 46, Issue 9, pp. 1884-1889 (SCI)

Yeau-Ren Jeng, and S. R. Peng, 2009, “Investigation into the Lateral Junction Growth of Single Asperity Contact Using Static Atomistic Simulations,” Applied Physics Letters, Vol. 94, Issue 16, 163103 (SCI)

Yeau-Ren Jeng, P. C. Tsai and Y. H. Liu, 2009, “Adsorbed Multilayer Effects on the Mechanical Properties in Nanometer Indentation Depth,” Materials Research Bulletin, Vol. 44, Issue 10, pp. 1995-1999 (SCI)

Yeau-Ren Jeng, T. T. Lin and D. B. Shieh, 2009, “Nanotribological Characterization of Tooth Enamel Rod Affected by Surface Treatment,” Journal of Biomechanics, Vol. 42, Issue 14, pp. 2249-2254 (SCI)

Yeau-Ren Jeng, P. C. Tsai, G. Z. Huang and I. L. Chang, 2009, “An Investigation into the Mechanical Behavior of Single-Walled Carbon Nanotubes under Uniaxial Tension Using Molecular Statics and Molecular Dynamics Simulations,” CMC: Computers, Materials, & Continua, Vol. 11, Issue 2, pp. 109-125 (SCI)

C. R. Das, S. Dhrar, Yeau-Ren Jeng, P. C. Tsai, H. C. Hsu, Baldev Raj, A. K. Bhaduri, S. K. Albert, A. K. Tyagi, L. C. Chen, and K. H. Chen, 2010, “Direct Observation of Amophization in Load Rate Dependent Nanoindentation Studies of Crystalline Si,” Applied Physics Letters, Vol. 96, Issue 25, 253113 (SCI)

Yeau-Ren Jeng ,Chien-Ping Mao,2010, “The effect of contaminants on the adhesion of the spatulae of a gecko,”Journal of Biosciences, Vol. 35, Issue 4 , pp. 595-603 (SCI)

Meng-Hung Lin, Yeau-Ren Jeng, Chang-Pin Chou , Hua-Chiang Wen , 2010, “Nanoscratch Characterization of GaN Epilayers on c- and a-Axis Sapphire Substrates,” Journal of Nanoscale Research Letters, Vol. 5, Issue 11, pp. 1812-1816 (SCI)

Yeau-Ren Jeng, Tsung-Ting Lin, Hsiu-Ming Hsu, Hsin-Ju Chang, Dar-Bin Shieh, 2011, “ Human Enamel Rod Presents Anisotropic Nanotribological Properties,” to be published in Journal of the Mechanical Behavior of Biomedical Materials(SCI)

Keynote Speaker of International Conferences

Yeau-Ren Jeng, 2010, “Nanomechanics of Asperity Contact: Multi-scale Perceptiive of Two Configurations,” Invited Lecture, The 12th International Congress on Mesomechanics, Taipei, Taiwan, June 21-26

Yeau-Ren Jeng, 2010, “Atomistic Investigation of Tribological Contacts,” Invited Keynote Speaker for Tribology Symposium of the Fifth International Conference Multiscale Materials Modeling, Freiburg, Germany, Oct. 4-8

Yeau-Ren Jeng, 2010, “Computations as Tools of Development and Discovery,”National Center for High-Performance Computing, Keynote Speaker, Hsinchu, Taiwan, Nov.4

Invited Speaker of International Conferences

Yeau-Ren Jeng, 2009, “A Multi-scale Perspective on Asperity Contact: A Study of Two Configurations,” Invited Speaker, Workshop on Multi-Scale Simulation, Academia Sinica, Taipei, Taiwan, April 6-7

Yeau-Ren Jeng, 2009, “Molecular Simulations of Asperity Contact: A Study of Two Configurations,” Invited Speaker, 6th Annual Taiwan/ US Air Force Nanoscience Workshop, California, USA, April 20-21

Yeau-Ren Jeng, 2009, “A Microscopic Elucidation on Contact Mechanics,” Invited Speaker, The 7th Cross-Strait Workshop on Nanoscience and Nanotechnology, Institute of Physics, Chinese Academy of Science, Guiyang, China, July 26-Aug. 1

Yeau-Ren Jeng, 2009, “A Multiscale Perspective of Asperity Contact: A Study of Two Configurations,” Invited Speaker, Workshop on Mesoscale Mechanics of Complex Materials, Vancouver, British Columbia, Canada, Nov. 2-3

Yeau-Ren Jeng, 2010, “Multi-scale Investigation of Asperity Contact: A Study of Nanomechanics,” Invited Speaker, The 7th Taiwan/U.S. Air Force Nanoscience Workshop, National Science and Technology Program for Nanoscience and Nanotechnology, Yilan,Taiwan, March 31-April 3

Yeau-Ren Jeng, 2010, “Multi-scale Perspective of Asperity Contact: Nanomechanics Investigation of Two Configurations,” Invited Speaker, International Workshop on Materials Behavior at the Micro- and Nano- Scale,

Xi' an, China, June 8-11

Yeau-Ren Jeng, 2010, “Lesson learned from Characterization of Nano-scale Mechanical Properties,” Invited Speaker, The 8th Cross-Strait Workshop on Nano Science and Technology, Hong Kong, China, Dec. 20-22